Running from Features: Optimized Evaluation of Inflationary Power Spectra

Hayato Motohashi[1] and Wayne Hu[1, 2]

[1]*Kavli Institute for Cosmological Physics, The University of Chicago, Chicago, Illinois 60637, USA*
[2]*Department of Astronomy and Astrophysics, University of Chicago, Chicago IL 60637, USA*
(Dated: October 10, 2018)

In models like axion monodromy, temporal features during inflation which are not associated with its ending can produce scalar, and to a lesser extent, tensor power spectra where deviations from scale-free power law spectra can be as large as the deviations from scale invariance itself. Here the standard slow-roll approach breaks down since its parameters evolve on an efolding scale ΔN much smaller than the efolds to the end of inflation. Using the generalized slow-roll approach, we show that the expansion of observables in a hierarchy of potential or Hubble evolution parameters comes from a Taylor expansion of the features around an evaluation point that can be optimized. Optimization of the leading-order expression provides a sufficiently accurate approximation for current data as long as the power spectrum can be described over the well-observed few efolds by the local tilt and running. Standard second-order approaches, often used in the literature, ironically are worse than leading-order approaches due to inconsistent evaluation of observables. We develop a new optimized next-order approach which predicts observables to 10^{-3} even for $\Delta N \sim 1$ where all parameters in the infinite hierarchy are of comparable magnitude. For models with $\Delta N \ll 1$, the generalized slow-roll approach provides integral expressions that are accurate to second order in the deviation from scale invariance. Their evaluation in the monodromy model provides highly accurate explicit relations between the running oscillation amplitude, frequency and phase in the curvature spectrum and parameters of the potential.

I. INTRODUCTION

In a general inflationary model, temporal scales that are not directly associated with the end of inflation leave their imprint in cosmological observables. For canonical single field models, these arise from features in the potential which leave the curvature and gravitational wave power spectra nearly scale invariant but no longer scale-free power laws. Current observations constrain deviations from scale-free power law spectra only as well as deviations from scale invariance itself [1]. Therefore these constraints only impact models with large features.

In the standard slow-roll approximation, the leading-order effect would be a running of the tilt of which the amplitude is quadratic in the small deviation from scale invariance. It is common to test for a finite value of such a parameter in data sets like the Planck CMB power spectra [1]. Yet the running of the tilt is only constrained at the $\sim 10^{-2}$ level, the same level as the tilt from scale invariance itself. Interpreting these constraints requires going beyond the standard approximation where slow-roll parameters are taken to be both nearly constant and strongly hierarchical (e.g. [2–5]). Using the standard second-order approach on such data, as is common in the literature (e.g. [1, 6–9]), can provide misleading results for models where the running of the tilt is not exactly constant or the potential purely cubic.

On the other hand, if the observed power spectra are well characterized by the local tilt and running of the tilt, which are the first two terms in a Taylor expansion of a continuous feature, then a slow-roll hierarchy still exists and can be used to predict observables accurately (cf. [10]). It is simply that the efolding scale of the feature ΔN, while still greater than unity, is much less than the number of efolds to the end of inflation.

In this paper, we use the generalized slow-roll (GSR) approach [10–16] to extend the validity of the standard slow-roll approximation. Here the deviations from scale invariance are only assumed to be small in amplitude not in temporal frequency. With GSR, we explore the relationship between features in the potential and the hierarchy of slow-roll parameters. Based on a temporal Taylor expansion, we develop optimized approaches for the evaluation of curvature and gravitational wave power spectra from inflation. We test these approaches in the axion monodromy model [17] where low frequency cases produce a slowly varying running of the tilt [18–20] and high frequency cases imprint oscillations in the power spectra [21, 22].

The paper is organized as follows. In §II, we review the GSR approach and iterate it to second order in the amplitude of deviations from scale invariance to describe power spectra in terms of integrals over the temporal history of inflation. We consider first order terms in §III and show how the Taylor expansion of the temporal history is related to observables and to the hierarchy of slow-roll parameters of the potential and Hubble evolution. Optimized evaluation of the leading-order Taylor term [11] provides predictions and inflation potential reconstructions that are accurate to next-to-leading order. These suffice for models with running of the tilt that is nearly constant across the observable scales. In §IV, we generalize the optimized approach to second order and an optimized next-to-leading-order approximation and contrast these approaches with the standard second-order approximation which inconsistently treats these evaluations. We illustrate these optimized evaluation techniques for monodromy in both the low and high frequency

regime in §V. We discuss these results in §VI and provide relationships between the various parameterizations in the Appendix.

II. GENERALIZED SLOW ROLL

The GSR approach is ideal for studying and extending the validity of the standard slow-roll approximation as it assumes only that the amplitude of deviations from a de Sitter expansion are small with no assumptions on their temporal frequency or equivalently on the smoothness of the potential [10, 11, 13, 14]. In this approach, we iteratively solve the exact Mukhanov-Sasaki equation for the evolution of the inflaton mode function or field fluctuation in the spatially flat gauge $\delta\phi = y/a\sqrt{2k}$

$$\frac{d^2y}{dx^2} + \left(1 - \frac{2}{x^2}\right)y = \left(\frac{f'' - 3f'}{f}\right)\frac{y}{x^2}, \quad (1)$$

to obtain the comoving curvature power spectrum

$$\Delta_{\mathcal{R}}^2 = \lim_{x \to 0} \left|\frac{xy}{f}\right|^2. \quad (2)$$

Here $' = d/d\ln\eta$, $x = k\eta$ and η is the (positive, decreasing) conformal time to the end of inflation and the deviations from de Sitter expansion are given by variations in

$$f^2 = \frac{8\pi^2 \epsilon_H}{H^2} (aH\eta)^2, \quad (3)$$

where the Hubble slow-roll parameter is defined by

$$\epsilon_H = -\frac{d\ln H}{dN} = \frac{1}{2}\left(\frac{d\phi}{dN}\right)^2, \quad (4)$$

with N as the (negative, increasing) number of efolds relative to the end of inflation.

The fundamental assumption in this approach is that the mode function y remains close to its de Sitter form

$$y_0(x) = \left(1 + \frac{i}{x}\right)e^{ix}, \quad (5)$$

and we will loosely refer to this property as requiring the amplitude of deviations from de Sitter or scale invariance encoded in f to be small (see [23–26] for exceptional cases). If so, we can take the formal Green function solution to Eq. (1),

$$y(x) = y_0(x) - \int_x^\infty \frac{du}{u^2}\frac{f'' - 3f'}{f}y(u)\text{Im}[y_0^*(u)y_0(x)], \quad (6)$$

replace $y \to y_0$ on the right-hand side and iteratively improve the solution.

To first order in the de Sitter deviations, this procedure results in [27]

$$\ln\Delta_{\mathcal{R}}^2(k) \approx I_0 = G(\ln x_*) + \int_{x_*}^\infty \frac{dx}{x}W(x)G'(\ln x), \quad (7)$$

where $x_* \ll 1$,

$$G = -2\ln f + \frac{2}{3}(\ln f)', \quad (8)$$

and

$$W(x) = \frac{3\sin(2x)}{2x^3} - \frac{3\cos(2x)}{x^2} - \frac{3\sin(2x)}{2x}. \quad (9)$$

While we assume a canonical scalar field throughout, all of the GSR-based results here and below can be readily generalized to $P(X, \phi)$ theories and the effective field theory that parameterizes them [16, 28].

The function W determines exactly how inflaton fluctuations freeze into curvature fluctuations as they pass the horizon. We can make the connection more explicit by integrating Eq. (7) by parts to obtain [27]

$$I_0 \approx -\int_0^\infty \frac{dx}{x}W'(x)G(\ln x). \quad (10)$$

Note that G is a function of time $\ln\eta$ alone and denoting it as a function of $\ln x$ is simply a convenient choice of its zero point for a given k. Scale dependence of the power spectrum arises only if $G' \neq 0$ and hence its value quantifies the deviations from de Sitter results. These typically must be

$$\bar{G}' = \mathcal{O}\left(\frac{1}{N}\right) \quad (11)$$

in order for features not to prematurely end inflation. The overbar here represents an average over several efolds and denotes the fact that only the integral of G' needs to be small or equivalently that transient effects do not necessarily end inflation. This average as we shall see is closely related to the average tilt of the curvature spectrum. In fact Eq. (10) is valid even if the inflaton potential contains discontinuities or delta function sources in G' where the local tilt and average tilt differ substantially. Given that $\lim_{x\to 0} W' = 0$, this form also conserves curvature fluctuations outside the horizon and gives a manifestly positive definite power spectrum, and it remains a controlled approximation for up to order unity deviations [14] unlike related variants [11, 13].

In particular, linearity in $\bar{G}'$ should not be conflated with the constancy of G'. If we define ΔN as the typical efolding scale of its variation, then

$$G'' = \mathcal{O}\left(\frac{1}{\Delta N}\right)G' = \mathcal{O}\left(\frac{1}{N\Delta N}\right) \quad (12)$$

rather than $1/N^2$ as the standard slow-roll approximation assumes by requiring that the only temporal feature during inflation be associated with its end. We shall show in §III that if $1 < \Delta N \ll |N|$, a slow-roll hierarchy of successively smaller derivative parameters still exists, but order counting needs to be generalized using a consistent Taylor expansion of G between observables. If $\Delta N \ll 1$, the hierarchy is inverted so that computing observables

requires resumming an infinite series or equivalently the direct integration of Eq. (10). In this regime observables depend on the continuous function G (see §V B), and model-independent approaches seek to reconstruct that function rather than measure a series of parameters [29–31].

These $\mathcal{O}(1/N\Delta N)$ effects should be distinguished from the true $1/N^2$ ones. In the GSR approximation, these come from terms that are quadratic in the deviation from de Sitter solutions G'. Iterating the Green function approach, we obtain [13, 14]

$$\Delta_{\mathcal{R}}^2 \approx e^{I_0}\left[\left(1 + \frac{1}{4}I_1^2 + \frac{1}{2}I_2\right)^2 + \frac{1}{2}I_1^2\right], \quad (13)$$

where the first-order term I_0 is defined in Eq. (7) and the second-order corrections are

$$I_1 = \frac{1}{\sqrt{2}}\int_0^\infty \frac{dx}{x}G'(\ln x)X(x),$$
$$I_2 = -4\int_0^\infty \frac{dx}{x}\left(X + \frac{1}{3}X'\right)\frac{f'}{f}\int_x^\infty \frac{du}{u^2}\frac{f'}{f}, \quad (14)$$

with

$$X(x) = \frac{3}{x^3}(\sin x - x\cos x)^2. \quad (15)$$

In the following sections we keep order counting in $1/N$ and $1/\Delta N$ distinct.

For tensor fluctuations, the same GSR approach holds with the replacement of f with

$$f_h^2 = \frac{2\pi^2}{H^2}(aH\eta)^2 \quad (16)$$

in the construction of the source G_h of the tensor fluctuations [15, 16]. With these substitutions, Eq. (13) then provides the tensor power spectrum in each polarization state $\ln \Delta_{+,\times}^2(k)$.

III. OPTIMIZED LEADING- AND FIRST-ORDER APPROXIMATION

Utilizing and extending the techniques of Ref. [11], we elucidate the conditions under which a slow-roll hierarchy of parameters for scalar and tensor power spectra observables exists and the relative size of terms in the series in §III A. In §III B, we show how the next-to-leading-order terms in the hierarchical expansion are generally large whenever running of the tilt is comparable to the deviations in the tilt itself but can be absorbed into an optimization in the time of fluctuation freeze-out consistently between observables. The resulting optimized leading-order description suffices for scalar and tensor spectra that can be described by a nearly constant running of the tilt even when it is of order the deviations from scale invariance represented by the tilt itself (cf. [10]). We relate this hierarchy to the Hubble slow roll parameters in §III C and to the potential slow-roll parameters in §III D.

A. Smoothness Hierarchy

The hierarchical structure of the slow-roll parameters stems from a smoothness assumption for the deviations from a de Sitter expansion. For any smooth source of deviations $G(\ln x)$ in the GSR formalism, we can Taylor expand its form around an epoch near horizon crossing $\ln x_f$ and integrate its effect term by term. The standard slow-roll approximation proceeds by assuming $\ln x_f = 0$ but we shall see there are advantages to tuning this evaluation point to make it correspond better to the freeze-out epoch. Note that a shift in this point corresponds to a shift in efolds of $\delta N \approx -\delta \ln x_f$.

For the first-order $\ln \Delta_{\mathcal{R}}^2 \approx I_0$ term of Eq. (10), this leads to

$$\ln \Delta_{\mathcal{R}}^2 \approx G(\ln x_f) + \sum_{p=1}^\infty q_p(\ln x_f)G^{(p)}(\ln x_f), \quad (17)$$

where $G^{(p)}$ denotes the pth derivative of G with respect to $\ln x$ and

$$q_p(\ln x_f) = -\frac{1}{p!}\int_0^\infty \frac{dx}{x}W'(x)\left(\ln \frac{x}{x_f}\right)^p. \quad (18)$$

These coefficients can be calculated using the generating function [11]

$$F(z, x_f) = -\int_0^\infty \frac{dx}{x}W'(x)\left(\frac{x}{x_f}\right)^z$$
$$= (2x_f)^{-z}\cos\left(\frac{\pi z}{2}\right)\frac{3\Gamma(2+z)}{(1-z)(3-z)}, \quad (19)$$

so that

$$q_p(\ln x_f) = \frac{1}{p!}\lim_{z\to 0}\frac{\partial^p F(z, x_f)}{\partial z^p}. \quad (20)$$

To clarify the dependence of these coefficients on $\ln x_f$, it is also useful to express $q_p(\ln x_f)$ in terms of the first term

$$q_1(\ln x_f) = \ln x_1 - \ln x_f, \quad (21)$$

where

$$\ln x_1 = \frac{7}{3} - \ln 2 - \gamma_E. \quad (22)$$

Here γ_E is the Euler-Mascheroni constant. Since

$$\frac{dq_p}{dq_1} = -\frac{dq_p}{d\ln x_f} = q_{p-1}, \quad (23)$$

q_p is a pth degree polynomial of q_1. Each degree introduces an extra constant of integration that is independent of $\ln x_f$. It is convenient to define these in terms of $q_p(\ln x_1)$ since $q_1(\ln x_1) = 0$. The higher coefficients become

$$q_p(\ln x_f) = \frac{q_1^p(\ln x_f)}{p!} + \sum_{n=0}^{p-2}\frac{q_{p-n}(\ln x_1)}{n!}q_1^n(\ln x_f). \quad (24)$$

The next two terms are thus given explicitly by

$$q_2(\ln x_f) = \frac{q_1^2(\ln x_f)}{2} + \frac{4 - 3\pi^2}{72}, \tag{25}$$

$$q_3(\ln x_f) = \frac{q_1^3(\ln x_f)}{6} + \frac{4 - 3\pi^2}{72} q_1(\ln x_f) + \frac{55}{81} - \frac{\zeta(3)}{3}.$$

We optimize the slow-roll approximation below by choosing $\ln x_f$ to set certain coefficients to zero. Equation (23) implies that setting $q_p(\ln x_f) = 0$ makes $q_{p+1}(\ln x_f)$ take on extremal values as a function of $\ln x_f$. Certain optimizations also have the benefit that the extremum is a minimum of $|q_{p+1}|$ and hence suppress the next correction.

Since

$$\frac{dG^{(p)}(\ln x_f)}{d\ln k} = -G^{(p+1)}(\ln x_f), \tag{26}$$

the tilt and the running of the tilt are given by

$$n_s - 1 \equiv \frac{d\ln\Delta_{\mathcal{R}}^2}{d\ln k} \approx -G'(\ln x_f) - \sum_{p=1}^{\infty} q_p G^{(p+1)}(\ln x_f),$$

$$\alpha \equiv \frac{dn_s}{d\ln k} \approx G''(\ln x_f) + \sum_{p=1}^{\infty} q_p G^{(p+2)}(\ln x_f), \tag{27}$$

with the obvious continuation to the running of each successive quantity. Since the q_p coefficients are fixed given a choice of $\ln x_f$ for all $\ln k$, we omit the $\ln x_f$ argument of q_p for clarity and where no confusion will arise we also do so below for compactness. A nearly constant tilt in $\ln k$ requires $|G''| \ll |G'|$, a nearly constant running $|G'''| \ll |G''|$, and each gains its next-to-leading-order correction from the q_1 term.

For tensor fluctuations, we similarly have [15, 16]

$$\ln\Delta_{+,\times}^2(k) \approx -\int_0^{\infty} \frac{dx}{x} W'(x) G_h(\ln x)$$

$$\approx G_h(\ln x_f) + \sum_{p=1}^{\infty} q_p G_h^{(p)}(\ln x_f), \tag{28}$$

which likewise determines the tensor tilt and running of the tilt

$$n_t \equiv \frac{d\ln\Delta_{+,\times}^2}{d\ln k} \approx -G_h'(\ln x_f) - \sum_{p=1}^{\infty} q_p G_h^{(p+1)}(\ln x_f),$$

$$\alpha_t \equiv \frac{dn_t}{d\ln k} \approx G_h''(\ln x_f) + \sum_{p=1}^{\infty} q_p G_h^{(p+2)}(\ln x_f). \tag{29}$$

For a sufficiently smooth $G(\ln x)$ and $G_h(\ln x)$, the series expansion of the power spectra will rapidly converge. Since

$$\lim_{p\to\infty} \frac{q_p}{q_{p-1}} = -\frac{1}{2}, \tag{30}$$

the criteria for convergence for the scalar power spectrum is

$$\lim_{p\to\infty} \left| \frac{G^{(p)}}{G^{(p-1)}} \right| < 2, \tag{31}$$

	LO/SO	OLO	ONO	GSR
p	0	1	2	∞
ΔN	$\gtrsim 50$	$\gtrsim$ few	$\gtrsim 1$	all
$\ln x_p$	0	1.06	0.22	–
q_1	1.06	0	0.84	–
q_2	0.21	-0.36	0	–
q_3	0.10	0.28	0.078	–

TABLE I. Slow-roll approximations are characterized by their order p in a temporal Taylor expansion which determines their applicability in describing features spanning ΔN efolds. Standard second-order (SO) approaches only improve on leading order (LO) by keeping $p > 0$ in some but not all observables. Optimized evaluation (OLO/ONO) achieves consistent pth order accuracy with only $p-1$ additional parameters by evaluating them at special values of $\ln x_f = \ln x_p$. The coefficients q_n for $n > p$ control the error from truncation. The GSR approximation forgoes the Taylor expansion for an integral approach.

and is similar for the tensor spectrum and tensor source G_h. The series is dominated by the first term for sufficiently small values for this ratio, with each successive term suppressed by the smoothness scale ΔN, $|G^{(p)}/G^{(p-1)}| = \mathcal{O}(\Delta N^{-1})$. Therefore, the Taylor expanded form above is applicable for features with $\Delta N \gtrsim 1$. For high frequency features where $\Delta N < 1/2$ and the convergence criteria are violated, the GSR integral formula must be developed on a case by case basis (see §V B for the monodromy example).

B. Optimized Leading vs. Next Order

We call an approximation scheme that just retains the GSR I_0 term and no corrections from the Taylor series, first order in deviations from scale invariance and leading order (LO) in the hierarchy. Namely,

$$\ln\Delta_{\mathcal{R}}^2 \approx G(\ln x_f),$$
$$n_s - 1 \approx -G'(\ln x_f),$$
$$\alpha \approx G''(\ln x_f), \qquad \text{(LO)} \tag{32}$$

and similarly for the tensor observables. One that adds $p = 1$ terms we call next(-to-leading)-order (NO) in the hierarchy. These distinctions still allow us to choose the evaluation epoch $\ln x_f$ which can be exploited to make a specific LO approximation as accurate as the generic NO approximation.

In the standard slow-roll approximation, one takes $\ln x_f = \ln x_0 \equiv 0$ and to NO

$$\ln\Delta_{\mathcal{R}}^2 \approx G(0) + q_1(0)G'(0),$$
$$n_s - 1 \approx -G'(0) - q_1(0)G''(0),$$
$$\alpha \approx G''(0) + q_1(0)G'''(0). \tag{33}$$

Here we have restored the $\ln x_f$ argument of q_n for clarity. Since $q_1(0) \approx 1.06$ (see Table I), if α is comparable to

$n_s - 1$ then the NO corrections are comparable to LO and are therefore required for accuracy.

On the other hand, since all observables follow this same Taylor series form, this NO approximation is equivalent to shifting the evaluation epoch by $q_1(0)$. This brings the evaluation point to

$$\ln x_1 = q_1(0) \approx 1.06, \qquad \text{(OLO)} \qquad (34)$$

which using Eq. (21) is equivalent to setting

$$q_1(\ln x_f) = q_1(\ln x_1) = 0. \qquad (35)$$

We call this the optimized leading order (OLO) approximation. By adopting this optimization, we gain all of the benefits of a next order approximation without any of the complexity. From this point forward, unless we specify otherwise, the LO approximation will refer to the *standard* LO approximation of $\ln x_f = 0$.

Beyond the NO approximation of Eq. (33), this shift does not resum the terms in the Taylor series since for $p > 1$

$$q_p(0) \neq \frac{q_1^p(0)}{p!} \qquad (36)$$

or equivalently for the OLO evaluation point $q_p(\ln x_1) \neq 0$. Furthermore $|q_2(\ln x_1)|$ is a local maximum of $|q_2(\ln x_f)|$ so that zeroing the NO correction comes at the expense of maximizing the next-to-NO correction. For a low frequency $\Delta N \gg 1$, i.e. for a strong hierarchy $|G^{(p)}/G^{(p-1)}| \ll 1$, this is a small price to pay. For $\Delta N \sim 1$, high accuracy requires going beyond the OLO optimization. In §IV we will optimize the NO approximation itself by zeroing the next-to-NO correction from q_2. We shall see that this has the added benefit that one can choose the solution that is a local minimum of $|q_3|$.

It is important to note that this series of optimizations is not equivalent to truncating at a fixed order in $1/\Delta N$. Since

$$G^{(p)} \equiv \frac{d^p G}{d \ln x^p} = \mathcal{O}\left(\frac{1}{N \Delta N^{p-1}}\right), \qquad (37)$$

dropping $\mathcal{O}(1/N\Delta N)$ would eliminate G'' in all observables including α and dropping $\mathcal{O}(1/N\Delta N^2)$ would retain the q_1 correction for $n_s - 1$ but not α. By truncating at the same order in the Taylor expansion of each observable, we have ensured that they are all consistently evaluated at the same effective epoch when the corrections are resummed. We shall see that this feature is crucial for ensuring consistency between observables. Table I summarizes the various approximations and their applicability.

Since derivatives with respect to $\ln \eta$ and $\ln k$ are interchangeable, the accuracy of this truncation at NO or equivalently OLO is directly related to the accuracy with which the power spectrum can be described by the local

tilt and running around a given pivot scale k_0

$$\ln \Delta_{\mathcal{R}}^2(k) \approx \ln A_s + [n_s(k_0) - 1] \ln \left(\frac{k}{k_0}\right)$$
$$+ \frac{\alpha(k_0)}{2} \ln^2 \left(\frac{k}{k_0}\right). \qquad (38)$$

If the observed power spectrum is a good fit to this form over at least the $\Delta N \sim$ few that are observationally well constrained, then OLO will also provide a good approximation. Omitted corrections are suppressed relative to OLO by $1/\Delta N^2$ for each observable.[*1] We shall quantify this consideration in §V A.

C. Hubble Slow Roll Parameters

Although the $G^{(p)}(\ln x_f)$ terms can themselves be thought of as the hierarchy of slow-roll parameters that are the most directly related to observables, it is useful to reexpress them in terms of the more familiar Hubble slow-roll parameters ϵ_H and

$$\delta_p \equiv \frac{1}{H^p \dot\phi} \left(\frac{d}{dt}\right)^{p+1} \phi, \qquad (39)$$

or equivalently derivatives of $\ln H$ with respect to efolds through the hierarchy relations

$$\frac{d \ln \epsilon_H}{dN} = 2(\epsilon_H + \delta_1),$$
$$\frac{d \ln \delta_p}{dN} = \frac{\delta_{p+1}}{\delta_p} + p\epsilon_H - \delta_1. \qquad (40)$$

Using these relations we can express $G^{(p)}$ in terms of the Hubble slow-roll parameters ϵ_H, δ_p as detailed in the Appendix. In particular, the hierarchy of $G^{(p)}$ derivatives is equivalent to the hierarchy of δ_p parameters. Equation (40) says that a hierarchical scaling with $|\delta_{p+1}/\delta_p| < 1$ requires the fractional change in δ_p per efold to be small in addition to $\epsilon_H, |\delta_1| \ll 1$. In particular, the Taylor expansion in $G^{(p)}$ becomes a summation over the hierarchy δ_p (see the Appendix)

$$G^{(p)} \approx (-1)^p \left(2\delta_p + \frac{2}{3}\delta_{p+1}\right) + \mathcal{O}\left(\frac{1}{N^2}\right), \qquad (41)$$

for $p \geq 2$. For order counting purposes

$$\epsilon_H, \delta_1 = \mathcal{O}\left(\frac{1}{N}\right), \quad \delta_p = \mathcal{O}\left(\frac{1}{N \Delta N^{p-1}}\right). \qquad (42)$$

Although our expressions for observables in terms of G are explicitly $\mathcal{O}(G') = \mathcal{O}(N^{-1})$ due to the linearity

---

[*1] The apparent contradiction with the power law example in Ref. [10] is due to numerical problems in their calculation [E. Stewart (private communication)]. Their feature model calculation is also in error.

of Eq. (17), we can choose whether or not to keep non-linear terms in the conversion of Hubble slow-roll parameters to G. Different choices will differ by $\mathcal{O}(N^{-2})$ and hence include a subset of second-order corrections arising from the evaluation of the first-order GSR term. Our convention will be to convert the OLO expression to $\mathcal{O}(N^{-1})$ in $\ln \Delta_{\mathcal{R}}^2$ and $n_s - 1$ but retain $\mathcal{O}(N^{-2})$ terms in α. This is to maintain backward compatibility with the standard slow-roll approximation where leading order for α is assumed to be $\mathcal{O}(N^{-2})$. We also drop terms that are $\mathcal{O}(N^{-2}/\Delta N)$. Thus, our leading-order expression spans the range of possibilities from $\Delta N \ll |N|$ to $\Delta N \sim |N|$, i.e. large to small running of the tilt. In this sense, our OLO approach is more general than the optimization introduced in Ref. [11] where $\Delta N \ll |N|$ is assumed.

With this convention the OLO scalar observables are

$$\ln \Delta_{\mathcal{R}}^2 \approx \ln \frac{H^2}{8\pi^2 \epsilon_H} - \frac{10}{3}\epsilon_H - \frac{2}{3}\delta_1 \Big|_{x=x_1}, \tag{43}$$

$$n_s - 1 \approx -4\epsilon_H - 2\delta_1 - \frac{2}{3}\delta_2 \Big|_{x=x_1}, \qquad \text{(OLO)}$$

$$\alpha \approx -2\delta_2 - \frac{2}{3}\delta_3 - 8\epsilon_H^2 - 10\epsilon_H \delta_1 + 2\delta_1^2 \Big|_{x=x_1}.$$

Here and below the notation $\big|_{...}$ applies to the whole expression. These differ from the standard slow-roll approximation in that δ_{p+1} terms are not dropped just because a lower-order δ_p appears.

Likewise the tensor observables become

$$\ln \Delta_{+,\times}^2 \approx \ln \frac{H^2}{2\pi^2} - \frac{8}{3}\epsilon_H \Big|_{x=x_1},$$

$$n_t \approx -2\epsilon_H \Big|_{x=x_1},$$

$$\alpha_t \approx -4\epsilon_H^2 - 4\epsilon_H \delta_1 \Big|_{x=x_1}, \qquad \text{(OLO)}. \tag{44}$$

These expressions for n_t and α_t are the same as the standard slow-roll expressions due to the lack of a running of n_t at linear order in ϵ_H and δ_n.

Since OLO self-consistently accounts for both running of the tilt and running of the running of the tilt by absorbing the next correction into the evaluation point, it is both a simpler and better approximation than keeping all $O(1/N^2)$ and $O(1/N\Delta N)$ terms in the standard slow-roll approximation as often used in the literature (e.g. [1, 6, 7]; see §V for tests). Note also that the standard approach is often phrased in terms of the Hubble flow parameters where δ_p and its hierarchy equation, Eq. (40), is replaced by

$$\frac{d \ln \epsilon_p}{dN} = \epsilon_{p+1}, \tag{45}$$

so that

$$\epsilon_1 \equiv \epsilon_H,$$
$$\epsilon_2 = 2(\epsilon_H + \delta_1),$$
$$\epsilon_2 \epsilon_3 = 4\epsilon_H^2 + 6\epsilon_H \delta_1 - 2\delta_1^2 + 2\delta_2. \tag{46}$$

While the two series are algebraically equivalent when all terms are kept, Hubble flow parameters are inconvenient for cases that lack a strong hierarchy [see Eq. (A17) and Fig. 14]. Equation (45) says that for ϵ_{p+1} to remain small, the fractional change in ϵ_p over an efold must be small. Hence order counting in powers of ϵ_p automatically conflates ΔN and N as Eq. (46) illustrates. For example in the cases considered in §V where the variations occur on $\Delta N \ll 1$, these parameters would have poles, whereas the δ_p do not.

D. Potential Slow Roll Parameters

We can likewise relate the $G^{(p)}$ hierarchy to the equivalent in derivatives of the potential. Using the exact background equations of motion for the inflaton and the expansion

$$(3 + \delta_1)H^2 \frac{d\phi}{dN} = -V^{(1)},$$
$$(3 - \epsilon_H)H^2 = V, \tag{47}$$

we can relate the derivatives of the potential to the Hubble slow-roll parameters

$$\mathcal{U} \equiv \left(\frac{V^{(1)}}{V}\right)^2 = 2\epsilon_H \frac{(1 + \delta_1/3)^2}{(1 - \epsilon_H/3)^2},$$

$$\mathcal{V}_1 \equiv \frac{V^{(2)}}{V} = \frac{\epsilon_H - \delta_1 - \delta_2/3}{1 - \epsilon_H/3}. \tag{48}$$

Note that to lowest order Eq. (48) gives $\mathcal{U} \approx 2\epsilon_H$ and $\mathcal{V}_1 \approx \epsilon_H - \delta_1 - \delta_2/3$. As shown in the Appendix, these imply $G' \approx 3\mathcal{U} - 2\mathcal{V}_1$. Likewise the series of higher-order derivatives with respect to efolds is replaced by higher-order derivatives of the potential with respect to the field

$$\mathcal{V}_p \equiv \left(\frac{V^{(1)}}{V}\right)^{p-1} \frac{V^{(p+1)}}{V}, \tag{49}$$

where $V^{(p)} \equiv d^p V/d\phi^p$. In the literature the first few parameters are also known as $\epsilon_V = \mathcal{U}/2$, $\eta_V = \mathcal{V}_1$, and $\xi_V = \mathcal{V}_2$. Terms that are quadratic in $\mathcal{U}, \mathcal{V}_p$ are higher order in the deviation from a de Sitter expansion. However, the relative size of the $\mathcal{V}_p$ parameters depends on the smoothness of the potential $V(\phi)$ just as that of δ_p depends on the smoothness of $H(N)$.

We explicitly carry out these conversions in the Appendix and outline the results relevant to the $\mathcal{O}(1/N)$ expansion here. Note that to leading order Eq. (47) provides the condition for a friction dominated roll or attractor solution,

$$\frac{d\phi}{dN} \approx -\frac{1}{3}\frac{V^{(1)}}{H^2} \approx -\frac{V^{(1)}}{V}, \tag{50}$$

which also converts the two senses of derivatives

$$\frac{d}{d \ln \eta} \approx \frac{V^{(1)}}{V} \frac{d}{d\phi}, \tag{51}$$

or

$$\frac{d\mathcal{U}}{d\ln\eta} \approx 0, \quad \frac{d\mathcal{V}_p}{d\ln\eta} \approx \mathcal{V}_{p+1}, \tag{52}$$

and thus

$$G^{(p)} \approx -2\mathcal{V}_p + \mathcal{O}(N^{-2}), \tag{53}$$

for $p \geq 2$. The Taylor series in $G^{(p)}$ has a one-to-one relationship to the same series in $\mathcal{V}_p$ (see the Appendix for details). The convergence criteria for the Taylor expansion in Eq. (31) likewise becomes a direct condition on the potential slow-roll parameters

$$\lim_{p\to\infty}\left|\frac{G^{(p)}}{G^{(p-1)}}\right| = \lim_{p\to\infty}\left|\frac{\mathcal{V}_p}{\mathcal{V}_{p-1}}\right| < 2. \tag{54}$$

We can interpret this condition by approximating

$$\frac{\mathcal{V}_p}{\mathcal{V}_{p-1}} \approx -\frac{d\phi}{dN}\frac{V^{(p+1)}}{V^{(p)}} \approx -\frac{d\ln V^{(p)}}{dN}. \tag{55}$$

Thus the convergence condition is that the fractional variation in $V^{(p)}$ experienced by the field across an efold is small.

Although the OLO approximation again follows directly from evaluating $G^{(p)}$ in terms of these parameters, it is useful to restore the general evaluation epoch $\ln x_f$ to clarify its relationship to the field position on the potential. Equations (17) and (27) become

$$\Delta_{\mathcal{R}}^2 \approx \frac{V}{12\pi^2\mathcal{U}}\left[1 + \left(3q_1 - \frac{7}{6}\right)\mathcal{U} - 2\sum_{p=1}^{\infty}q_p\mathcal{V}_p\right],$$

$$n_s - 1 \approx -3\mathcal{U} + 2\mathcal{V}_1 + 2\sum_{p=1}^{\infty}q_p\mathcal{V}_{p+1},$$

$$\alpha \approx -2\mathcal{V}_2 - 2\sum_{p=1}^{\infty}q_p\mathcal{V}_{p+2} - 6\mathcal{U}^2 + 8\mathcal{U}\mathcal{V}_1, \tag{56}$$

where the potential terms are evaluated at the field position $\phi(\ln x_f)$ which we will write as $\ln x_f$ as shorthand notation. In this language, optimization of $\ln x_f$ is equivalent to optimization of the field position at which to evaluate the potential parameters. From the field position $\ln x_f = \ln x_0 = 0$, a shift in evaluation point to $\ln x_1 = q_1(0)$ causes a shift of

$$\delta\phi \approx -\frac{V^{(1)}}{V}\delta N \approx \frac{V^{(1)}}{V}q_1(0) \tag{57}$$

or a change in potential parameters

$$\delta V \approx V^{(1)}\delta\phi \approx \mathcal{U}Vq_1(0),$$

$$\delta\mathcal{U} \approx 2\frac{V^{(1)}}{V}(\mathcal{V}_1 - \mathcal{U})\delta\phi \approx 2\mathcal{U}(\mathcal{V}_1 - \mathcal{U})q_1(0),$$

$$\delta\mathcal{V}_p \approx \frac{V}{V^{(1)}}\mathcal{V}_{p+1}\delta\phi \approx \mathcal{V}_{p+1}q_1(0) \tag{58}$$

that cancel the NO corrections in the hierarchy. In fact starting from an arbitrary $\ln x_f$ we can define

$$\tilde{\mathcal{V}}_p(\ln x_f) \equiv \mathcal{V}_p(\ln x_f) + q_1(\ln x_f)\mathcal{V}_{p+1}(\ln x_f)$$
$$\approx \mathcal{V}_p(\ln x_1). \tag{59}$$

For the OLO choice, $\tilde{\mathcal{V}}_p(\ln x_1) = \mathcal{V}_p(\ln x_1)$, and for alternate $\ln x_f$, $\tilde{\mathcal{V}}_p(\ln x_f)$ differs from $\mathcal{V}_p(\ln x_1)$ only by next-to-NO corrections. $\tilde{\mathcal{V}}_n$ will be useful for comparing higher-order approximations in §IV. In fact for an arbitrary order we could define $\tilde{\mathcal{V}}_p \equiv \mathcal{V}_p + \sum q_n\mathcal{V}_{n+p}$ to absorb the appropriate number of correction terms into an effective potential parameter.

Thus the OLO approximation simply amounts to shifting the evaluation point in field space by the same amount for all observables. Maintaining this consistency condition is important in testing models. Aside from this evaluation point, the OLO approximation ($\ln x_f = \ln x_1$) takes the same form as the standard LO approximation ($\ln x_f = 0$),

$$\Delta_{\mathcal{R}}^2 \approx \frac{V}{12\pi^2\mathcal{U}}\left(1 - \frac{7}{6}\mathcal{U}\right),$$

$$n_s - 1 \approx -3\mathcal{U} + 2\mathcal{V}_1,$$

$$\alpha \approx -2\mathcal{V}_2 - 6\mathcal{U}^2 + 8\mathcal{U}\mathcal{V}_1, \quad \text{(O/LO)}. \tag{60}$$

Though identical in form, the standard approximation assumes $\mathcal{V}_2$ is $\mathcal{O}(N^{-2})$ making α suppressed with respect to $n_s - 1$ and absent in its leading-order prediction, not because of resummation to a new evaluation point but because of its truncation at $\mathcal{O}(N^{-1})$. Again, the advantage of this OLO is that not only is it as simple as the standard LO slow-roll prescription, but it consistently incorporates the NO corrections that run the tilt and run the running of the tilt. Corrections to it are suppressed by $\mathcal{O}(1/\Delta N^2)$.

We shall see that the same is not true for approaches that correct for evolution at a fixed order in powers of $\Delta N \sim N$ as is often used in the literature (e.g. [3, 8, 9]). For instance if α is of order $n_s - 1$, the standard second-order approach is really only appropriate for strictly constant α or equivalently a purely cubic potential where the cubic term is large but no higher terms are important. Importantly, in OLO we absorb the effect of the quartic term $\mathcal{V}_3$ in the optimized evaluation of α to correct for the running of its value between horizon crossing and freeze-out. In the second-order approach, tilt is run to the freeze-out point, but running is not. One would then infer an incorrect relationship between the derivatives of the potential and hence potentially incorrectly falsify a true model that is not purely cubic from observations. Thus, a second-order approach is both more complicated and less general than the OLO approach. We illustrate this in §V A for the monodromy example.

For tensor fluctuations, conversion of $G_h^{(p)}$ to the po-

tential parameters gives

$$\Delta_{+,\times}^2(k) \approx \frac{V}{6\pi^2}\left[1 - \frac{7}{6}\mathcal{U}\right],$$
$$r \approx 8\mathcal{U},$$
$$n_t \approx -\mathcal{U},$$
$$\alpha_t \approx -2\mathcal{U}^2 + 2\mathcal{U}\mathcal{V}_1, \qquad \text{(O/LO)} \qquad (61)$$

where the only NO correction is in the power spectrum itself,

$$\delta\Delta_{+,\times}^2(k) = \frac{V}{6\pi^2}q_1\mathcal{U}, \qquad \text{(NO)}. \qquad (62)$$

Here again OLO has the same accuracy as NO since $q_1(\ln x_1) = 0$. In particular the consistency relation $r \approx -8n_t$ remains unchanged regardless of the evaluation point $\ln x_f$.

Finally, the OLO approximation provides a simple inverse relationship between the observables r, n_s and α and the potential parameters

$$\mathcal{U} \approx \frac{r}{8},$$
$$\mathcal{V}_1 \approx \frac{n_s - 1}{2} + \frac{3r}{16},$$
$$\mathcal{V}_2 \approx -\frac{\alpha}{2} + \frac{1}{4}(n_s-1)r + \frac{3r^2}{64}, \qquad \text{(OLO)}. \quad (63)$$

Even if r is not accurately measured, strong upper limits where $r \ll 8|1 - n_s|/3$ allow a reconstruction of $\mathcal{V}_1$ and $\mathcal{V}_2$.

Equivalently, those observables allow a local reconstruction of the potential to cubic order around the field value where $x(\phi_0) = x_1$

$$\frac{V}{V_0} \approx 1 + \sqrt{\mathcal{U}}(\phi-\phi_0) + \frac{\mathcal{V}_1}{2}(\phi-\phi_0)^2 + \frac{\mathcal{V}_2}{6\sqrt{\mathcal{U}}}(\phi-\phi_0)^3. \quad (64)$$

The potential amplitude V_0, or the energy scale of inflation, can likewise be determined from measuring $\Delta_{+,\times}^2$ or equivalently $\Delta_\mathcal{R}^2$ and r as is well known.

IV. OPTIMIZED NEXT- AND SECOND-ORDER APPROXIMATION

The OLO approximation of the previous section is accurate at first order in the deviations from scale invariance $\mathcal{O}(1/N)$ and next-to-leading order (NO) in a hierarchy of slow-roll parameters separated by ΔN, the temporal scale of features during inflation. For cases where $\Delta N \sim 1$ and the hierarchy is weakly convergent or if higher accuracy is desired for future observations, we can generalize this approach. In §IV A we consider next-to-NO in the hierarchy and an $\mathcal{O}(1/N^2)$ in the de Sitter deviations. In §IV B, we develop a new optimized NO (ONO) approximation that retains the simplicity of the NO approximation. This also allows us to contrast OLO and ONO with the standard second order (SO) approach which conflates ΔN and N in §IV C.

A. General Expression

In terms of the hierarchy of slow-roll parameters, the next-to-NO approximation involves keeping terms to order $p = 2$ in the Taylor expansion of G in Eq. (17)

$$I_0 \approx G(\ln x_f) + \sum_{p=1}^{2} q_p G^{(p)}(\ln x_f). \qquad (65)$$

To also include all $\mathcal{O}(1/N^2)$ effects, we evaluate the second-order terms I_1 and I_2 from Eq. (14). In these corrections, G' and f'/f can be taken as constants evaluated at $\ln x_f$ as their evolution introduces terms of $\mathcal{O}(1/N^2\Delta N)$ which we omit. Combining these pieces, we obtain

$$\ln \Delta_\mathcal{R}^2(k) \approx G(\ln x_f) + q_1 G'(\ln x_f) + q_2 G''(\ln x_f)$$
$$+ \frac{\pi^2}{8}[G'(\ln x_f)]^2 - 4\left[\frac{f'}{f}(\ln x_f)\right]^2. \quad (66)$$

The same expression is valid for tensors with the appropriate replacements as before.

Since the variation in $\ln k$ of the last two I_1 and I_2 terms in Eq. (66) is itself $\mathcal{O}(1/N^2\Delta N)$, we do not include their impact on n_s or α. The only $\mathcal{O}(1/N^2)$ terms that appear for those quantities come from the nonlinear relationship between $G^{(p)}$ and slow-roll parameters. This justifies our inclusion of such terms in α in the OLO approximation since there are no further corrections from intrinsically second-order GSR effects.

As shown in the Appendix, in terms of the potential slow-roll parameters we obtain

$$\Delta_\mathcal{R}^2 \approx \frac{V}{12\pi^2\mathcal{U}}\left[1 + \left(3q_1 - \frac{7}{6}\right)\mathcal{U} - 2q_1\mathcal{V}_1 - 2q_2\mathcal{V}_2\right.$$
$$+ \left(3q_2 - \frac{2}{3}q_1 - \frac{103}{9} + \frac{3\pi^2}{2}\right)\mathcal{U}^2$$
$$+ \left(-4q_2 + \frac{2}{3}q_1 + 15 - 2\pi^2\right)\mathcal{U}\mathcal{V}_1$$
$$+ \left.\left(4q_2 - \frac{2}{3}q_1 - \frac{13}{3} + \frac{2\pi^2}{3}\right)\mathcal{V}_1^2\right],$$
$$n_s \approx 1 - 3\mathcal{U} + 2\mathcal{V}_1 + 2q_1\mathcal{V}_2 + 2q_2\mathcal{V}_3$$
$$+ \left(6q_1 - \frac{17}{6}\right)\mathcal{U}^2 - \left(8q_1 - \frac{5}{3}\right)\mathcal{U}\mathcal{V}_1 + \frac{2}{3}\mathcal{V}_1^2,$$
$$\alpha \approx -2\mathcal{V}_2 - 2q_1\mathcal{V}_3 - 2q_2\mathcal{V}_4 - 6\mathcal{U}^2 + 8\mathcal{U}\mathcal{V}_1, \qquad (67)$$

for the scalar expression and

$$\Delta_{+,\times}^2 \approx \frac{V}{6\pi^2}\left[1 + \left(q_1 - \frac{7}{6}\right)\mathcal{U}\right.$$
$$+ \left(-q_2 + \frac{4}{3}q_1 - \frac{8}{3} + \frac{\pi^2}{6}\right)\mathcal{U}^2$$
$$\left.+ \left(2q_2 - 2q_1 + \frac{17}{9}\right)\mathcal{U}\mathcal{V}_1\right],$$
$$r \approx 8\mathcal{U} - 16q_1\mathcal{U}(\mathcal{U} - \mathcal{V}_1),$$
$$n_t \approx -\mathcal{U} + \left(2q_1 - \frac{5}{2}\right)\mathcal{U}^2 - 2(q_1 - 1)\mathcal{U}\mathcal{V}_1,$$
$$\alpha_t \approx -2\mathcal{U}(\mathcal{U} - \mathcal{V}_1), \qquad (68)$$

for the tensor expression. These are the master equations for all next-to-NO in the hierarchy and second order in $1/N$ approximations. They of course also include lower-order approximations such as LO, OLO and SO with the appropriate zeroing of terms.

B. Optimized Evaluation

We can again optimize the evaluation epoch $\ln x_f$ to make the optimized NO approximation as accurate as a general next-to-NO approximation. We therefore take $q_2(\ln x_2) = 0$ in Eq. (25) and pick the solution that minimizes the next correction $|q_3|$,

$$q_2(\ln x_2) \equiv 0,$$
$$q_1(\ln x_2) = \frac{\sqrt{3\pi^2 - 4}}{6} \approx 0.84,$$
$$\ln x_2 = \ln x_1 - q_1(\ln x_2) \approx 0.22, \quad \text{(ONO).} \quad (69)$$

We call the evaluation of Eqs. (67) and (68) with these values the optimized next-order (ONO) approximation. Note that this has the effect of zeroing the highest $\mathcal{V}_p$ term in each observable.

For a strong hierarchy $\Delta N \gg 1$, despite the shift in the actual evaluation point to $\ln x_2$, observables remain effectively evaluated at $\ln x_1$ since

$$I_0 = G(\ln x_2) + q_1(\ln x_2)G'(\ln x_2) + \dots$$
$$= G(\ln x_2) + (\ln x_1 - \ln x_2)G'(\ln x_2) + \dots$$
$$= G(\ln x_1) - \frac{1}{2}(\ln x_1 - \ln x_2)^2 G''(\ln x_1) + \dots$$
$$= G(\ln x_1) + q_2(\ln x_1)G''(\ln x_1) + \dots \qquad (70)$$

where $\dots$ represents $G^{(3)}$ terms and higher. Evaluation at $\ln x_2$ simply increases the accuracy by including the first correction to this approximation. Since $\ln x_1$ is a maximum of $|q_2|$ this correction can become important for $\Delta N \sim 1$. Furthermore $\ln x_2$ is a minimum of $|q_3|$ and so even the $G^{(3)}$ error is minimized in ONO (see Table I).

In terms of the reconstruction of $\mathcal{U}, \mathcal{V}_1, \mathcal{V}_2$ from n_s, α, r the system is no longer closed due to the appearance of $q_1\mathcal{V}_3$ in α. As in the case of I_0 above, this term represents the leading-order effect of a shift in the evaluation

of $\mathcal{V}_2$ back to $\phi(\ln x_1)$ from $\phi(\ln x_2)$. We can therefore define instead the reconstructed parameters as the $\tilde{\mathcal{V}}_p$ of Eq. (59) which can equally well be predicted from any given model for comparison. Moreover in the quadratic terms the difference between employing $\mathcal{V}_p$ and $\tilde{\mathcal{V}}_p$ is at most $\mathcal{O}(1/N^2\Delta N)$ which we neglect. Thus the master equation can be written entirely in terms of $\tilde{\mathcal{V}}_p$. Iterating the inversion we obtain

$$\mathcal{U} \approx \frac{r}{8} - \frac{q_1}{8}(n_s - 1)r - \frac{q_1}{64}r^2,$$
$$\tilde{\mathcal{V}}_1 \approx \frac{n_s - 1}{2} + \frac{3r}{16} - \frac{(n_s - 1)^2}{12}$$
$$+ \left(\frac{q_1}{16} - \frac{11}{96}\right)(n_s - 1)r + \left(\frac{3q_1}{128} - \frac{7}{768}\right)r^2,$$
$$\tilde{\mathcal{V}}_2 \approx -\frac{\alpha}{2} + \frac{1}{4}(n_s - 1)r + \frac{3r^2}{64}, \qquad \text{(ONO),} \qquad (71)$$

for the potential reconstruction.

C. Standard Second Order

We can also contrast the OLO and ONO approximations with the standard second-order approach. The standard second-order approach is not simply a choice of $\ln x_f = 0$ in the master equations. By conflating ΔN with N, it truncates at a fixed order in both. In other words it assumes $\mathcal{V}_p = \mathcal{O}(1/N^p)$ and so in the $\mathcal{O}(1/N^2)$ expansion,

$$\mathcal{V}_3, \mathcal{V}_4, \dots = 0, \qquad \text{(SO),}$$
$$q_1 \approx 1.06, \quad q_2 \approx 0.21 \qquad (72)$$

in Eqs. (67) and (68). Thus, the standard second-order (SO) approximation implicitly assumes that the potential is cubic in form (see the Appendix for the relationship to the second-order Hubble flow approximation). Since truncation at a fixed $\mathcal{V}_p$ is not the same as truncation at a fixed order in the Taylor expansion, this means that different observables are effectively evaluated at an inconsistent $\ln x_f$ or field position. We shall see that this makes SO an even worse approximation than OLO for cases where $\Delta N \ll |N|$ and the potential is not cubic.

In particular, dropping $q_1\mathcal{V}_3$ terms in α but keeping $q_1\mathcal{V}_2$ terms in $n_s - 1$ leads to the reconstruction

$$\mathcal{U} \approx \frac{r}{8} - \frac{q_1}{8}(n_s - 1)r - \frac{q_1}{64}r^2,$$
$$\mathcal{V}_1 \approx \frac{n_s - 1}{2} + \frac{3r}{16} + \frac{q_1}{2}\alpha - \frac{(n_s - 1)^2}{12}$$
$$- \left(\frac{3q_1}{16} + \frac{11}{96}\right)(n_s - 1)r - \left(\frac{3q_1}{128} + \frac{7}{768}\right)r^2,$$
$$\mathcal{V}_2 \approx -\frac{\alpha}{2} + \frac{1}{4}(n_s - 1)r + \frac{3r^2}{64}, \qquad \text{(SO),} \qquad (73)$$

which is not simply a redefinition of q_1 in Eq. (71).

In particular α now appears in the formula for $\mathcal{V}_1$. For a purely cubic potential, these differences simply reflect

a different expansion point ϕ_0 for the reconstruction in Eq. (64). However for a potential that contains quartic corrections, the SO reconstruction can lead to inconsistencies between the parameters $\{\mathcal{U}, \mathcal{V}_1, \mathcal{V}_2\}$ that do not simply reflect evaluation at a different field value for the potential. We now turn to an illustrative example of such a model.

V. MONODROMY CASE STUDY

Axion monodromy inflation [17] provides a well-motivated theoretical model where the various approximation schemes discussed in the previous sections can be tested. The monodromy potential is the sum of a smooth and oscillatory part

$$V(\phi) = \bar{V}(\phi) + \delta V(\phi), \tag{74}$$

for which we take the simplest case

$$\begin{aligned}\bar{V}(\phi) &= \lambda\phi, \\ \delta V(\phi) &= \Lambda^4 \cos\left(\frac{\phi}{f} + \theta\right).\end{aligned} \tag{75}$$

Depending on the frequency of this oscillation, the curvature power spectrum may gain a large local running of the tilt [18, 20] or high frequency features for which the slow-roll parameters have an inverted hierarchy and lose their ability to characterize observables directly [21].

In §V A, we study the low frequency case and test the accuracy of the LO, OLO, ONO and SO approximations. We develop optimized GSR approximations for the high frequency case in §V B, extending results of Ref. [21] for second-order corrections in the large amplitude limit as well as establishing the connection of the running amplitude, frequency, and phase of the oscillation to parameters of the potential.

A. Low Frequency Oscillations

In the low frequency regime, the slow-roll parameters are hierarchical and yet the running of tilt can be large and nearly constant across the well-measured few efolds of the cosmic microwave background (CMB) and large-scale structure. In this case, the OLO and ONO slow-roll expressions should provide a good approximation for observables whereas we have argued that the standard SO expressions do not.

For tests of these approximations, we choose the parameters of the potential such that the smooth piece provides a power spectrum amplitude and tilt of the right order at some fiducial scale k_0,

$$\begin{aligned}\bar{\Delta}_{\mathcal{R}}^2(k_0) &= \bar{A}_s = 2.5 \times 10^{-9}, \\ \bar{n}_s &= 0.97,\end{aligned} \tag{76}$$
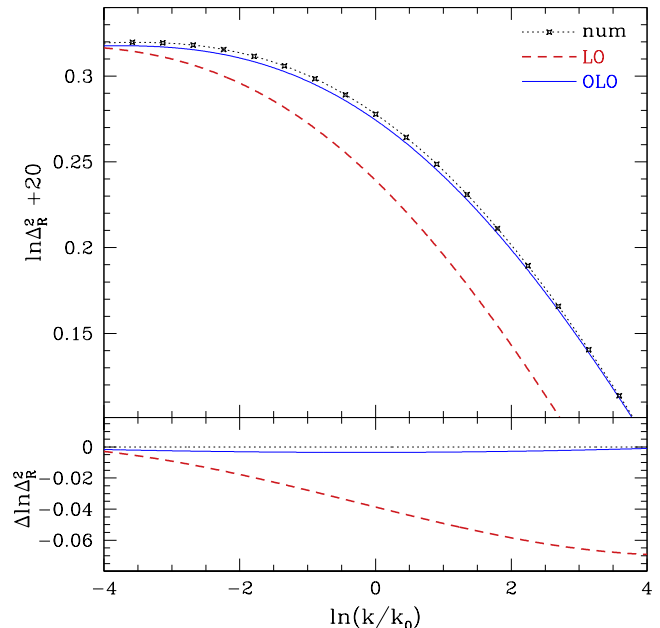

FIG. 1. Low frequency $\omega = 1/3$ oscillations in the curvature power spectrum $\Delta_{\mathcal{R}}^2$ under the leading-order (LO) and optimized leading-order (OLO) approximations. While the LO approximation introduces a large error in the power spectrum compared to numerics, the OLO results show that they can be corrected by simply shifting the relationship between $\ln k$ and ϕ. Here the amplitude of the oscillation is set to $\alpha_{\max} = -0.01$.

which determines

$$\begin{aligned}\phi_0 &= \sqrt{\frac{3}{1 - \bar{n}_s}}, \\ \lambda &= \frac{12\pi^2}{\phi_0^3}\bar{A}_s.\end{aligned} \tag{77}$$

As shown by the OLO approximation, fluctuations freeze out at

$$k_0\eta(\phi_0) = x_1 \approx 2.89, \tag{78}$$

which provides a conversion between k_0 and ϕ_0 which we use as a definition throughout. The parameter f determines the frequency of the oscillation and thus the separation between terms in the slow-roll hierarchy. Since

$$\left|\frac{\mathcal{V}_p}{\mathcal{V}_{p-1}}\right| \approx \frac{1}{f\phi_0} = \frac{|d\phi/dN|}{f} \equiv \omega \ll 1, \tag{79}$$

we fix f by a choice of $\omega \sim \Delta N^{-1}$. Given Eq. (54), the series expansion in p converges if $\omega < 2$. Thus in the low frequency regime $\omega \ll 1$, the optimized slow-roll approach should be a good approximation.

We set the phase of the oscillation so that α is at an extrema $\alpha_{\max}$ at k_0,

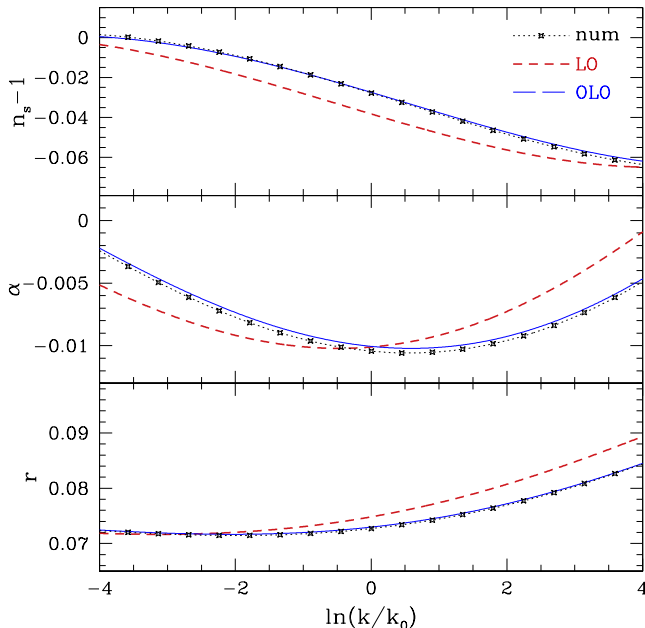$$\theta = \frac{\pi}{2} - \text{Mod}(\phi_0/f, 2\pi), \tag{80}$$

FIG. 2. Low frequency $\omega = 1/3$ oscillations in n_s, α and r under the LO and OLO approximations as in Fig. 1. The OLO approximation again provides an excellent approximation that corrects the shift in the LO results even in this case where ω, the hierarchical separation between α and $n_s - 1$, is not much less than unity.

for low frequency oscillations. Finally we set the amplitude of the oscillations Λ^4 by relating it to the running of the tilt at the k_0 extrema

$$\Lambda^4 = -\frac{1}{2}\lambda\phi_0^2 f^3 \alpha_{\max}. \tag{81}$$

In practice we choose $\alpha_{\max} = -0.01$ in our examples. Since Λ^4 increases as $\omega \to 0$ at fixed $\alpha_{\max}$ and $n_s - 1$, higher-order terms in δV eventually become important. Therefore, we use $\alpha_{\max}$ simply as a proxy for choosing Λ^4 rather than associating it with the actual value of α at k_0. Likewise, $\bar{A}_s$ and $\bar{n}_s$ also receive higher-order corrections and are used here simply to set parameters.

By solving the exact Mukhanov-Sasaki equation (1) with Bunch-Davies initial conditions (5), we can compare the power spectra observables to the various slow-roll approximations and integral approaches.

We start by considering an example with $\omega = 1/3$. In Fig. 1, we compare the standard LO and OLO approximation of Eq. (60) against the numerical calculation for the curvature power spectrum $\Delta_{\mathcal{R}}^2$. The OLO approximation reproduces the numerical calculation at the 10^{-3} level, while the LO approximation misestimates the power spectrum by a considerable amount. On the other hand, we know analytically that the two differ simply in that the power spectrum is shifted by $\Delta \ln k \approx -\ln x_1$. Since the relationship between k and ϕ depends on the physics of reheating, this type of error just introduces an
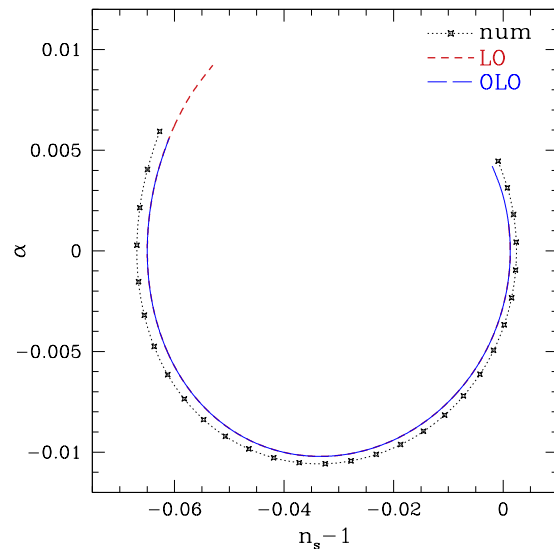

FIG. 3. Low frequency $\omega = 1/3$ oscillation trajectories in the n_s-α plane under the LO and OLO approximations as in Fig. 1. Both LO and OLO trajectories are good approximations to the numerical results emphasizing that the LO results differ simply in the evaluation point along the trajectory, parametrically evaluated here for the same range in observed wavenumber k.

efold shift in those inferences rather than on the shape of the potential.

These considerations apply to n_s, α, and r as illustrated in Fig. 2. The OLO approximation is highly accurate with differences from the numerics at the 10^{-3} level or less, whereas the LO results are all shifted by the same amount as the power spectrum.

This joint shift of all observables means that for the LO approximation all four observables are consistent with arising from the same potential as would be inferred from the better OLO approximation. For example, we show trajectories in the n_s-α plane in Fig. 3. The difference between the two approximations now appears simply as a different starting and ending point on the same trajectory.

The importance of consistency becomes clear when comparing potential reconstruction between the LO and OLO approximations in Eq. (63). In Fig. 4, we show reconstruction using the exact, numerical results for n_s, α, and r as a function of $\ln k$ as if they were precisely measured from data. Again the OLO approximation is highly accurate for reconstruction, whereas the LO approximation shows a shift in ϕ due to the change in the evaluation epoch

Consistency in the evaluation epoch between observables leads to consistency in the potential reconstruction. In Fig. 5, we show trajectories in the $\mathcal{V}_1$-$\mathcal{V}_2$ plane. The difference between the LO and OLO approximations is again the starting and ending point on the trajectory. Both approximations would reconstruct potentials that
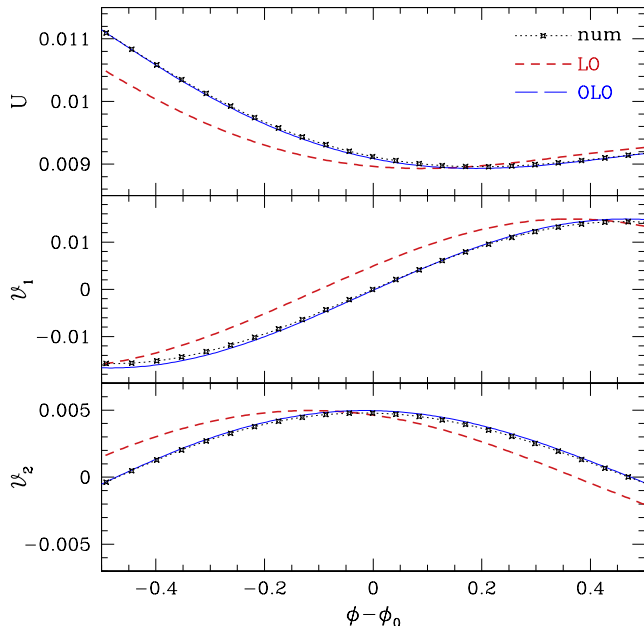
FIG. 4. Low frequency $\omega = 1/3$ potential reconstruction in $U, \mathcal{V}_1, \mathcal{V}_2$ under the LO and OLO approximations as in Fig. 1. Here the numerical results for n_s, α, r are used in each case. The OLO approximation is accurate at the 10^{-3} level whereas the LO approximation produces a systematic but consistent shift in field position.

FIG. 5. Low frequency $\omega = 1/3$ oscillation trajectories in the $\mathcal{V}_1$-$\mathcal{V}_2$ plane under the LO and OLO approximations as in Fig. 1. Both LO and OLO trajectories are good approximations to the numerical results emphasizing that the LO results err simply in the evaluation point along the trajectory, parametrically evaluated here for the same range in observed wavenumber k.

were consistent with the true potential at the same level of accuracy. Though the values of $\mathcal{V}_1$ and $\mathcal{V}_2$ that they recover do differ, they are consistent with a shifted evaluation on the potential.

This should be contrasted with the standard second-order (SO) approximation. In Fig. 6, we show the SO and ONO approximations for $\Delta_{\mathcal{R}}^2$ from Eqs. (67) and (68). Both approximations do an excellent job of correcting residual errors in the LO and OLO approximations in the power spectrum itself. For n_s, α, r, Fig. 7 shows that ONO further improves the error in their predictions from OLO to well below 10^{-3}. Residual errors are largest for α due in large part to the neglect of the $\mathcal{O}(1/N^2\Delta N)$ term $8q_1\mathcal{U}\mathcal{V}_2$ in Eq. (67) and would decrease for smaller choices of ω. On the other hand, SO only corrects LO for $n_s - 1$ and r leaving the large fractional error in α that was present at LO.

Ironically this means that the SO approximation performs worse than LO in an important sense. In Fig. 8, we highlight the problem for the trajectories in the n_s-α plane. Unlike the LO approximation, the SO approximation predicts pairs of these observables that are strongly inconsistent with the true trajectory.

Likewise for potential reconstruction, the ONO approximation improves the reconstruction to better than the 10^{-4} level. In fact by defining fully self-consistent corrected potential parameters $\tilde{\mathcal{V}}_n$ from Eq. (59), 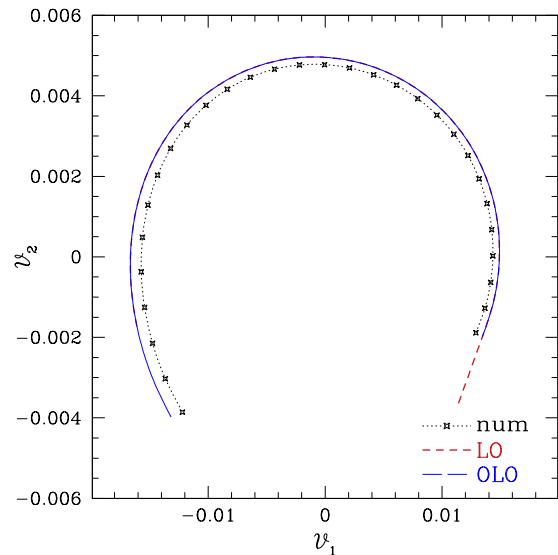reconstruction is actually more accurate than the power spectrum prediction since it absorbs $\mathcal{O}(1/N^2\Delta N)$ terms into the definition. On the other hand, while the SO approximation corrects the shift of the LO approximation in $\mathcal{U}$ and $\mathcal{V}_1$, it does not for $\mathcal{V}_2$ as shown in Fig. 9. The consequence is that in the $\mathcal{V}_1$-$\mathcal{V}_2$ plane shown in Fig. 10 the SO approximation reconstructs points that are not consistent with being anywhere on the trajectory of the true potential. This can lead to incorrect falsification of the true model from observations.

Perhaps surprisingly, the OLO and ONO approximations still perform well for $\omega = 1$ where all terms in the infinite $\mathcal{V}_n$ series are of the same order. This is related to the fact that the Taylor series still converges, albeit slowly, for even larger values up to $\omega < 2$. In Fig. 11, we show their predictions for $n_s - 1$, α and r. For the precision of current measurements, the OLO approximation actually still suffices. For higher precision measurements, the ONO approximation now makes relatively important corrections to the scalar observables and performs well at the 10^{-3} level.

Finally, the accuracy of the OLO and ONO approximations are directly related to the accuracy with which the local tilt and running describe the global power spectrum across the observed efolds through Eq. (38). In Fig. 12, we show that in the $\omega = 1/3$ case where the OLO approximation suffices this approximation is very accurate over a large range in efolds. For the $\omega = 1$ case, the approximation only holds for the central ~ 4 efolds and likewise the ONO corrections to OLO become important. Thus, if the observations are a good fit to the local model, then
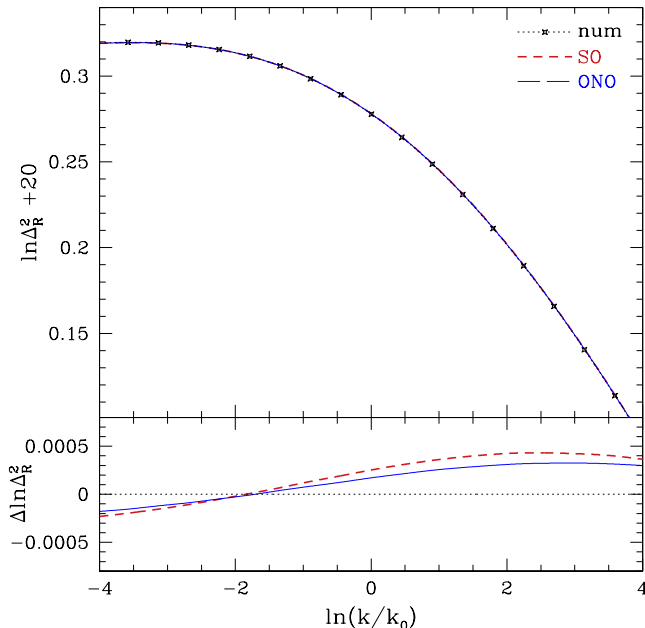
FIG. 6. Low frequency $\omega = 1/3$ oscillations in the curvature power spectrum $\Delta_\mathcal{R}^2$ under the standard second-order (SO) and optimized next-order (ONO) approximations. In both cases, the second-order corrections are sufficient to correct errors in Fig. 1 to below the 10^{-3} level (bottom panel).

FIG. 7. Low frequency $\omega = 1/3$ oscillations for the error in n_s, α and r relative to numerics under the SO and ONO approximations. ONO further improves OLO but SO only corrects LO in n_s and r compared with Fig. 2. α remains shifted in SO and breaks the internal consistency of the observables.

OLO is a good approximation, and ONO provides the means to improve its accuracy if necessary in the future. If the local model is a bad fit to the data, then $\Delta N \lesssim 1/2$ (or $\omega \gtrsim 2$), and no slow-roll hierarchy of parameters can describe the spectrum accurately.

B. High Frequency Oscillations

For $\omega > 2$, the slow-roll hierarchy does not converge with a finite number of terms. Nonetheless, the GSR expansion remains valid so long as the deviations from scale invariance, controlled by the amplitude not the frequency of the oscillation, remains small. We must, however, evaluate the GSR integrals in Eqs. (7) and (14) directly. Given that in the high frequency limit $\mathcal{V}_p$ increases with p, we can no longer naively use their relationships with $G^{(p)}$ given in the Appendix. Reference [14] showed that, even in the high frequency limit,

$$G' = 3\mathcal{U} - 2\mathcal{V}_1 + \epsilon_H \mathcal{O}(G') + \mathcal{O}(\delta_1^2). \qquad (82)$$

We can therefore establish the leading-order connection to the potential in the usual way. Namely for the oscillatory part,

$$\delta G = 3\frac{\delta V}{\bar{V}} - 2\frac{\delta V^{(1)}}{\bar{V}^{(1)}}. \qquad (83)$$

Moreover, this leading-order result remains valid even for large amplitude, high frequency oscillations since G'
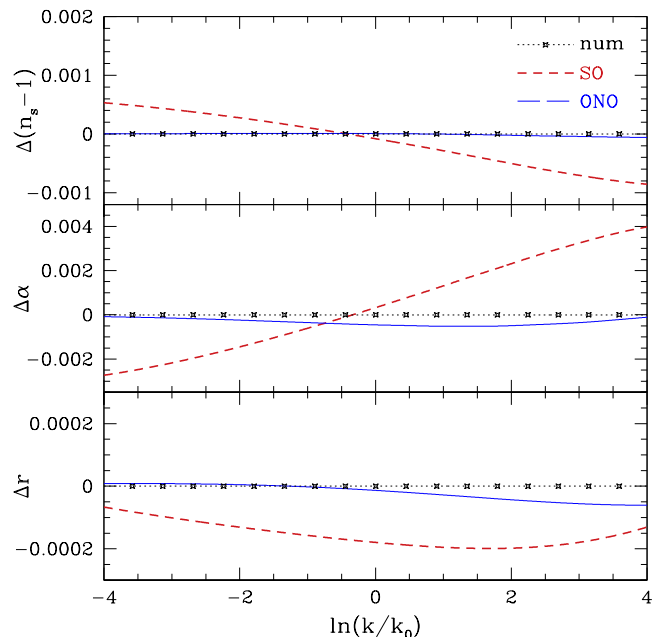
is linear in the highest derivative term $V^{(2)}$ (or δ_2) and hence linear in Λ^4 in that limit. This extended validity will be important in the consideration of quadratic terms below. It can be demonstrated by integrating $\delta G'$ assuming that the field rolls according to the smooth potential. Even large amplitude high frequency oscillations give highly suppressed effects on the field position which we can neglect.

Under this approximation for the roll, we can convert field position to time relative to some fiducial evaluation point η_* as

$$\phi \approx \phi_* + \sqrt{2\bar{\epsilon}_H}\ln(\eta/\eta_*) \approx \phi_* + \frac{1}{\phi_*}\ln(x/k\eta_*) \qquad (84)$$

to obtain the leading-order contribution from the oscillations $\delta \ln \Delta_\mathcal{R}^2(k) \approx \delta I_0(k)$, where

$$\delta I_0 \approx -\frac{2\Lambda^4}{\lambda f}\int_0^\infty \frac{dx}{x}W'(x)\left[\sin\left(\omega_*\ln x + \psi\right)\right.$$
$$\left. + \frac{3f}{2\phi_*}\cos\left(\omega_*\ln x + \psi\right)\right], \qquad (85)$$

with $\omega_* = (f\phi_*)^{-1}$ and

$$\psi(k) = \frac{\phi_*}{f} - \omega_*\ln(k\eta_*) + \theta. \qquad (86)$$

As in the optimized slow-roll calculations, the epoch η_* and the associated field value ϕ_* can be optimized to
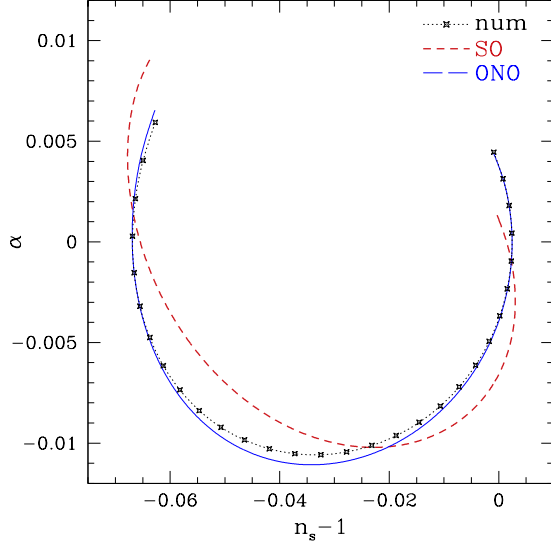
FIG. 8. Low frequency $\omega = 1/3$ oscillation trajectories in the n_s-α plane under the SO and ONO. ONO improves OLO but SO is worse than the LO (cf. Fig. 3 and also Fig. 14 for the second-order Hubble flow result).

make the approximations as accurate as possible for a given k. It does not have to coincide with the fixed η_0 and ϕ_0, associated with horizon crossing for k_0.

We can evaluate both terms in the integral using Eq. (19),

$$\int_0^\infty \frac{dx}{x} W'(x) e^{i\omega_* \ln x}$$
$$= -2^{-i\omega_*} \cosh\left(\frac{\pi\omega_*}{2}\right) \frac{3\Gamma(2 + i\omega_*)}{(1 - i\omega_*)(3 - i\omega_*)}$$
$$= \sqrt{\frac{9\pi\omega_* \coth(\pi\omega_*/2)}{2(9 + \omega_*^2)}} e^{i(\pi/2 - \beta)}. \quad (87)$$

The phase factor $\beta(\omega_*)$ can be expressed exactly in terms of the Γ function formula. Note that it takes on simple limiting forms

$$\lim_{\omega_* \to 0} \beta = \frac{3\pi}{2} - \omega_* \ln x_1,$$
$$\beta_\infty \equiv \lim_{\omega_* \to \infty} \beta = \omega_*[1 - \ln(\omega_*/2)] - \frac{\pi}{4}. \quad (88)$$

Here $\ln x_1 \approx 1.06$ is the same factor that enters into the OLO approximation for reasons that will be clear below. The large ω_* limit corresponds to the resonant or stationary phase solution of $x = \omega_*/2$ for the phase factor $2x - \omega_* \ln x$ [21]. To clarify the connection between these limits, it is useful to have a simple approximation to the exact $\beta(\omega_*)$ and we find that

$$\beta(\omega_*) \approx \beta_\infty + \frac{7\pi}{4} \frac{1}{\sqrt{1 + 1.59\omega_*^{0.92} + \omega_*^2}} \quad (89)$$

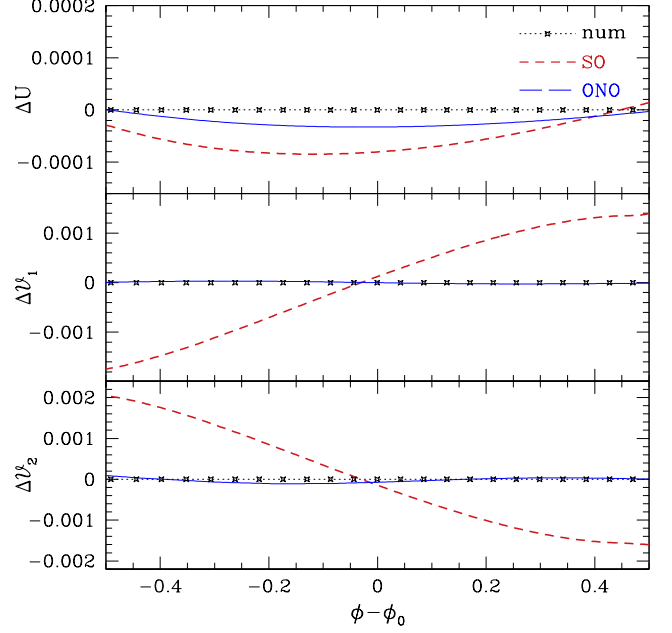to better than 0.03 accuracy everywhere.

FIG. 9. Low frequency $\omega = 1/3$ potential reconstruction error in $\mathcal{U}, \mathcal{V}_1, \mathcal{V}_2$ under the SO and ONO approximations. ONO reconstructs the potential to extremely high accuracy ($\sim 10^{-4}$), but SO corrects only $\mathcal{U}$ and $\mathcal{V}_1$ compared with Fig. 4 leaving $\mathcal{V}_2$ with large fractional errors. For ONO, we plot $\delta\tilde{\mathcal{V}}_1$, $\delta\tilde{\mathcal{V}}_2$.

Putting these results together, we obtain

$$\delta I_0(k) = -A\left[\cos(\psi - \beta) - \frac{3f}{2\phi_*} \sin(\psi - \beta)\right], \quad (90)$$

where

$$A = \frac{12\Lambda^4}{\lambda f \sqrt{1 + (3f\phi_*)^2}} \sqrt{\frac{\pi}{8} f\phi_* \coth\left(\frac{\pi}{2f\phi_*}\right)}. \quad (91)$$

This should be compared to the result from Ref. [21],

$$\delta\Delta_\mathcal{R}^2 = \bar{A}_s \left(\frac{k}{k_0}\right)^{\bar{n}_s - 1} A \cos\left[\omega \ln(k/k_0) + \varphi\right], \quad (92)$$

where φ is considered a free phase parameter. Since this form is primarily used for the purpose of fitting a functional form for the deviations to data, in this comparison differences in the form are more important than those in the association of A, ω, and φ with parameters in the potential. On the other hand, our treatment has the advantage of preserving all of those relations.

For example, Ref. [21] ignores corrections of order $f/\phi_* \approx 2\epsilon_H/\omega_*$ as they are not relevant for high frequency oscillations, but these may be absorbed into a redefinition of amplitude and phase. More importantly they take

$$\delta \ln \Delta_\mathcal{R}^2 \approx \frac{\delta\Delta_\mathcal{R}^2}{\bar{\Delta}_\mathcal{R}^2} \quad (93)$$
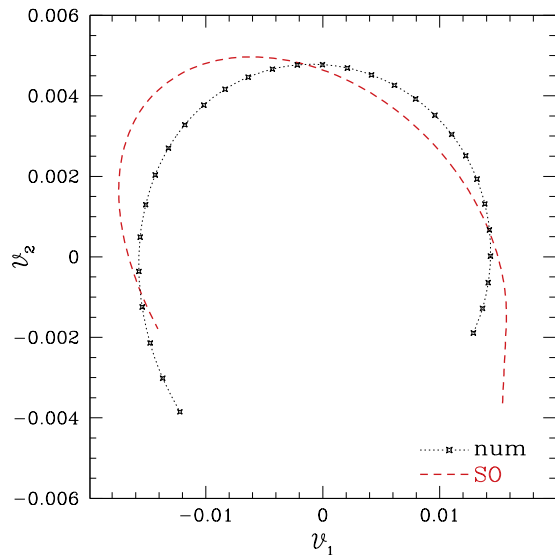
FIG. 10. Low frequency $\omega = 1/3$ oscillation trajectories in the $\mathcal{V}_1$-$\mathcal{V}_2$ plane under the SO approximation as in Fig. 1. SO is worse than LO (cf. Fig. 5) and can lead to an incorrect falsification of the true model.

which is valid in the $|A| \ll 1$ limit but causes differences that cannot be reabsorbed into fits at large A. Note that Eq. (92) does not guarantee a positive definite power spectrum.

In terms of the phase, Eq. (92) defines only the k dependence rather than the absolute relationship between φ and θ given by our treatment. The dependence of the phase on k in Eq. (86) is consistent with Eq. (92) if we choose the evaluation epoch as $\eta_* = 1/k_0$,

$$\psi \approx \frac{\phi_*}{f} - \omega_* \ln(k/k_0) + \theta. \qquad (94)$$

The advantage of the more general Eq. (90) is that we are not required to do so. Using a fixed evaluation epoch omits the evolution of quantities like $\bar{\epsilon}_H$ between that epoch and the true freeze-out epoch which depends on k. In the more refined treatment of Ref. [22], these effects are absorbed into a running or drift of the frequency. Note that this type of running does not invalidate our use of the slow-roll approximation in Eq. (84) which only requires constant $\bar{\epsilon}_H$ during freeze-out of a given k rather than across many efolds of k and hence N space.

We can instead parallel and extend our low frequency treatment by allowing the freeze-out epoch for the oscillatory piece δV to depend on k in potentially a different way than for $\bar{V}$. We start by reexamining the low frequency case where the two freeze-out epochs should be the same. Indeed, if we take the evaluation point as $k\eta_* = x_1$, the $\ln x_1$ phase shift in β in Eq. (88) cancels with the opposite shift in ψ in Eq. (86) so that

$$\lim_{\omega_* \to 0} (\psi - \beta) = \frac{\phi_*}{f} + \theta + \frac{\pi}{2}, \quad k\eta_* = x_1. \qquad (95)$$

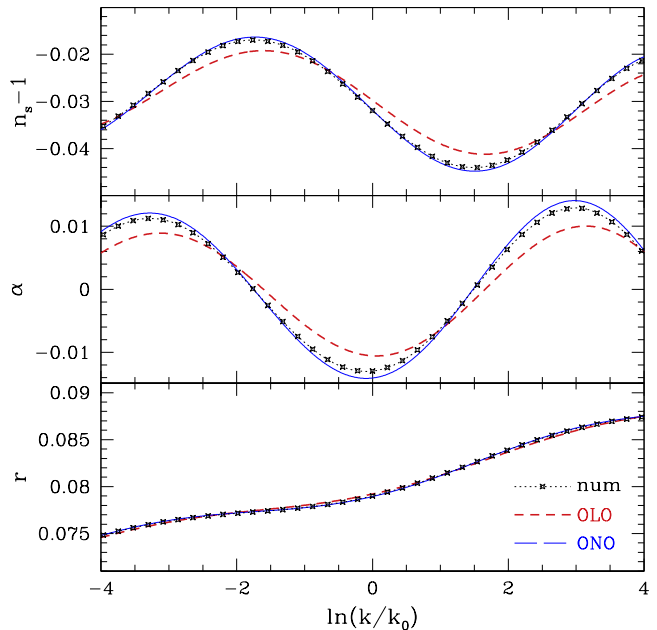FIG. 11. Intermediate frequency $\omega = 1$ oscillation in n_s, α, and r under the OLO and ONO approximations. OLO is still sufficiently accurate for current measurements, but ONO provides notable corrections and preserves 10^{-3} accuracy in observables.

Equation (90) in the $\omega \ll 1$ limit is then exactly the OLO approximation using Eq. (83):

$$\delta I_0 \approx \delta G|_{x=x_1}, \quad \text{(OLO)} \qquad (96)$$
$$\approx \frac{2\Lambda^4}{\lambda f} \left[\sin\left(\frac{\phi_*}{f} + \theta\right) + \frac{3f}{2\phi_*} \cos\left(\frac{\phi_*}{f} + \theta\right) \right].$$

Note that here ϕ_* is a function of k due to the optimized evaluation, and the explicit dependence can either be directly computed given the background solution or characterized by the running of the frequency from some central value at k_0 [22].

For high frequency oscillations $\omega \gg 1$, we increase accuracy by shifting the evaluation point η_* to the stationary phase point

$$\lim_{\omega_* \to \infty} (\psi - \beta) = \frac{\phi_*}{f} - \omega_* + \theta + \frac{\pi}{4}, \quad k\eta_* = \frac{\omega_*}{2}. \qquad (97)$$

Optimized evaluation again means that $\phi_*(k)$ is given by the solution to

$$k\eta(\phi_*) = \frac{\omega_*}{2} = \frac{1}{2f\phi_*}. \qquad (98)$$

To cover both low and high frequency cases, we can combine the two freeze-out criteria as

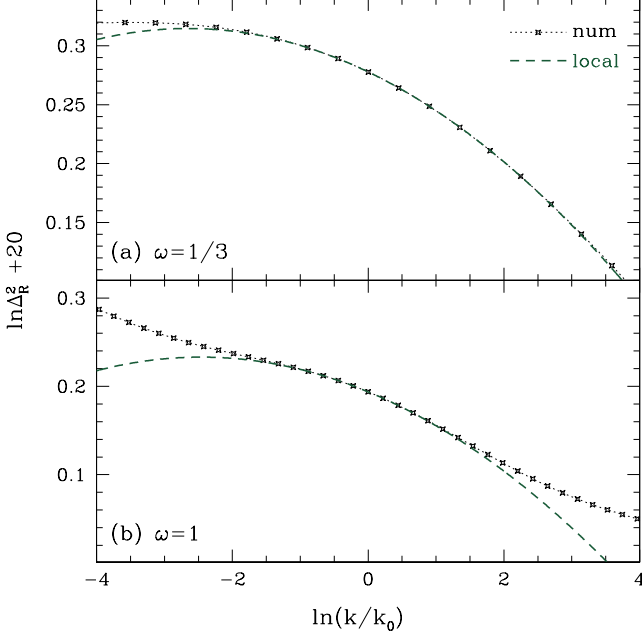$$k\eta_* = \max\left(x_1, \frac{\omega_*}{2}\right). \qquad (99)$$

FIG. 12. Local, $n_s - \alpha$ parameterization of the power spectrum from Eq. (38) compared to numerics for the low and intermediate frequency cases. Accuracy of the local approximation is directly related to the hierarchical structure of the slow-roll parameters and hence that of the OLO truncation of the hierarchy. For $\omega = 1/3$ both suffice, whereas for $\omega = 1$ both require correction from higher terms in their respective Taylor series.
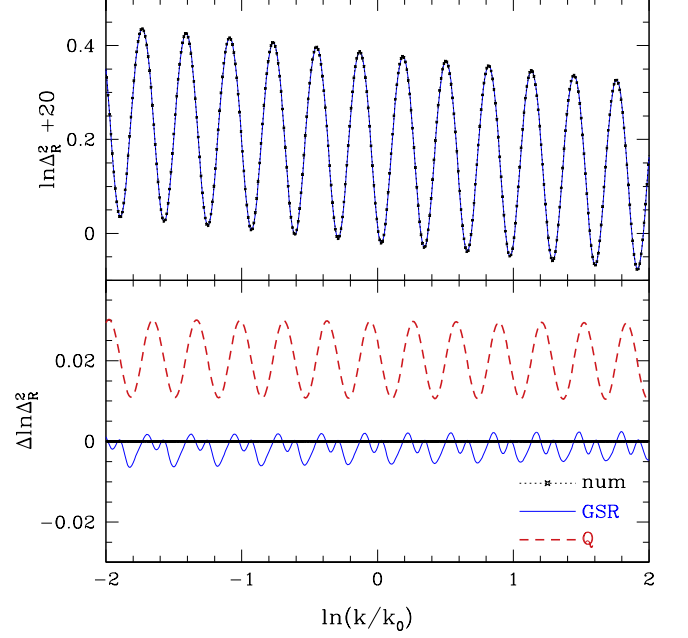

FIG. 13. High frequency $\omega = 20$ oscillation in the curvature power spectrum $\Delta_{\mathcal{R}}^2$ under the analytic GSR integral approximation as compared with numerical calculations for a model with $A \sim 0.2$ amplitude oscillations (top). Differences are less than 10^{-2} with a significant correction coming from the quadratic terms (Q) which mainly change the phase and amplitude of the oscillation as well as shift the normalization parameter $\ln \bar{A}_s$ (bottom).

For the second-order corrections in the $\omega \ll 1$ limit, the ONO approximation applies and captures all terms. In the opposite limit of $\omega \gg 1$, quadratic terms in A can be more relevant since a large amplitude oscillation does not produce large changes to the well-constrained average tilt and running. In this large amplitude and frequency limit, the dominant second-order correction is due to I_1 [14] where a similar resonance occurs in the stationary phase approximation. Thus, the oscillatory part of the power spectrum is well approximated by

$$\delta \ln \Delta_{\mathcal{R}}^2 \approx \delta I_0 + 2\bar{I}_1 \delta I_1 + \delta I_1^2, \quad \text{(GSR)} \tag{100}$$

where the smooth and oscillatory parts of I_1 are given by

$$\bar{I}_1 = \frac{\pi}{2\sqrt{2}}(1 - \bar{n}_s), \tag{101}$$

and

$$\delta I_1 = \frac{1}{\sqrt{2}} \int_0^\infty \frac{dx}{x} \delta G'(\ln x) X(x). \tag{102}$$

Repeating the same steps as for I_0, we have integrals

that can be evaluated using

$$\int_0^\infty \frac{dx}{x} X'(x) e^{i\omega_* \ln x}$$
$$= -2^{-i\omega_*} i \sinh\left(\frac{\pi\omega_*}{2}\right) \frac{3\Gamma(2 + i\omega_*)}{(1 - i\omega_*)(3 - i\omega_*)}$$
$$= -\sqrt{\frac{9\omega_* \pi \tanh(\pi\omega_*/2)}{2(9 + \omega_*^2)}} e^{-i\beta}, \tag{103}$$

to obtain

$$\delta I_1 = \frac{A}{\sqrt{2}} \tanh\left(\frac{\pi\omega_*}{2}\right) \left[\sin(\psi - \beta) + \frac{3f}{2\phi_*} \cos(\psi - \beta)\right]. \tag{104}$$

Note that the δI_1^2 correction contains squared or $2\omega_*$ frequency contributions that cannot fully be absorbed into the form of Eq. (92). However to quadratic order in A, the combination of the I_0 and I_1 differences in form between Eqs. (100) and (92) can be absorbed into a redefinition of $\bar{A}_s$, A and the oscillation phase for $\omega \gg 1$. To see this note that, aside from the phase $\psi - \beta$, these quadratic differences are given by

$$Q = \frac{\delta I_0^2}{2} + 2\bar{I}_1 \delta I_1 + \delta I_1^2 \tag{105}$$

and $\sqrt{2}\delta I_1$ and δI_0 are related by a phase shift of

$\pi/2$ such that their squares sum to a constant since $\tanh(\pi\omega_*/2) \to 1$.

As an example, we choose $\omega = 20$ and $\Lambda^4 = 1.78 \times 10^{-13}$ which gives $A(k_0) \approx 0.2$. Other parameters are set as in the low frequency case. We use the ONO approximation to determine $\bar{A}_s$, $\bar{n}_s$, and $\bar{\alpha}$ for the smooth potential and add its contribution using Eq. (38) to compare the total

$$\ln \Delta_{\mathcal{R}}^2 = \ln \bar{\Delta}_{\mathcal{R}}^2 \Big|_{\text{ONO}} + \delta \ln \Delta_{\mathcal{R}}^2 \qquad (106)$$

to numerical results. Note that, by implementing the ONO approximation, where $\bar{V}$ is evaluated at $k\eta(\phi_2) = x_2$, we use two field positions ϕ_* and ϕ_2 for each k which allows us to simultaneously optimize for the oscillatory and smooth parts of the potential.

In Fig. 13, we show that even for this large amplitude oscillation, Eq. (100) is accurate to better than 10^{-2} without any adjustment to the phase, frequency or amplitude of oscillations. Note that, as expected, the quadratic terms in Q, while significant in establishing the good agreement with numerics, takes the form of a constant plus an oscillatory piece of the same frequency as the leading-order contribution. Thus, it can be absorbed into a redefinition of parameters in Eq. (92) and the dependence of the oscillation phase $\psi - \beta$ on k. For even larger values of the amplitude A, this is no longer possible and so accurate expressions will require calculations to cubic and higher order in A

VI. DISCUSSION

By utilizing the GSR approximation, we have provided a systematic study of the evaluation and interpretation of power spectra where a relatively large local running arises from features in the potential. This approach assumes only that the average deviation from scale invariance is small and associated with the number of efolds to the end of inflation as $1/N$. The frequency of temporal features $1/\Delta N$ can be much larger than $1/N$. We introduced the GSR slow-roll hierarchy parameters $G^{(p)}$ which are directly related to observables and elucidate their relation to the standard hierarchies of parameters in the potential and Hubble flow. This parameterization works for $P(X, \phi)$ models as well with a suitable generalization of the conformal time to the sound horizon.

For models with $1 < \Delta N \ll N$, a slow-roll hierarchy of parameters still exists, but the running of the tilt α is only smaller than $n_s - 1$ by a factor of ΔN not N. In these models, the leading-order slow-roll calculation gains relatively large corrections since a large running implies that the slow-roll parameters are not constant. Instead the calculation and interpretation of such models proceeds by Taylor expanding the temporal evolution. This series converges rapidly as long as $\Delta N \gtrsim$ few, and this condition also guarantees that observable power spectra are well characterized by the local tilt and running across

the well-measured few efolds of the CMB and large scale structure.

In fact next-to-leading-order corrections in the Taylor series of each observable can be consistently reabsorbed into an optimized temporal evaluation of leading-order terms. This is because the first Taylor correction just represents a shift in the epoch of fluctuation freeze-out to about an efold before horizon crossing. The advantage of this OLO approach is that the analysis of observables proceeds exactly in the same way as a standard leading-order analysis and only the interpretation in terms of their correspondence to the inflationary model differs. For the interpretation of current data fits to constant tilt and running of the tilt, this simple approach suffices in accuracy. In terms of potential reconstruction it recovers a local cubic expansion evaluated consistently at the optimized field point.

Contrast this with a common approach in the literature that attempts to correct for the evolution with a second-order expansion under the assumption that $\Delta N \sim N$. In this case the tilt is corrected for evolution between horizon crossing and freeze-out but the running of the tilt, which is assumed to be intrinsically second order, is not. In this case, the observables are effectively evaluated at inconsistent epochs. Potential reconstruction from a second-order approach likewise produces inconsistencies which could potentially lead to an incorrect falsification of the true model from the observations. For models with large running it can only be consistently applied to a purely, rather than locally, cubic potential. Ironically then the second-order analysis provides a more complicated but less general approach compared with the leading-order analysis as we explicitly demonstrate using a low frequency axion monodromy model.

For even higher accuracy, we can keep both $1/N^2$ terms and optimized next-to-leading-order terms in the hierarchy. This ONO approach leads to better than 10^{-3} accuracy in observables and potential reconstruction even for $\Delta N \sim 1$ where all of the infinite hierarchy of parameters have the same magnitude.

Finally for $\Delta N \ll 1$, the slow-roll parameters possess an inverted hierarchy and lose their utility for predicting observables. Even in this case the GSR approach provides accurate predictions as long as the amplitude of deviations from time translation invariance is small regardless of the frequency of temporal features. Likewise the technique of optimizing the epoch of evaluation can be generalized to establish precise relationships between the potential parameters and observables.

We test this GSR approach with axion monodromy models in the high frequency limit and provide expressions that are accurate to second order in the amplitude and optimized in the temporal evaluation. The optimized approach also provides the direct relationship between parameters of the potential and phenomenological template fits to the running phase, frequency and amplitude of oscillations in the power spectrum used in the literature. For sufficiently large amplitude deviations and/or

future high precision measurements, relating power spectrum features to potential parameters requires going beyond the second order calculations presented here. We leave such considerations and their impact on interpreting observables to a future work.

Appendix A: Parameter Relations

To relate the three different parameterizations of the slow-roll hierarchy $G^{(p)}$, $\{\epsilon_H, \delta_p\}$ and $\{\mathcal{U}, \mathcal{V}_p\}$ used in the main text, we establish here the relationship between the GSR, Hubble slow-roll, and potential slow-roll approaches.

We expand expressions to $\mathcal{O}(1/N^2)$ under the assumption that

$$
\{\epsilon_H, \mathcal{U}\} = \mathcal{O}\left(\frac{1}{N}\right),
$$

$$
\{G^{(p)}, \delta_p, \mathcal{V}_p\} = \mathcal{O}\left(\frac{1}{N\Delta N^{p-1}}\right). \qquad \text{(A1)}
$$

with $1 \ll \Delta N \leq |N|$. Unlike the standard slow-roll approximation, we therefore keep terms that are $\mathcal{O}(1/N\Delta N^p)$ but still drop those that are $O(1/N^2\Delta N^p)$ for $p \geq 1$. For example we keep $\mathcal{V}_2$ and $\mathcal{U}\mathcal{V}_1$ but omit $\mathcal{U}\mathcal{V}_2$.

The relationship between the GSR and Hubble slow-roll variables involves the conversion between conformal time and efold

$$
\frac{dN}{d\ln\eta} = -aH\eta. \qquad \text{(A2)}
$$

This quantity can be parameterized by using Eqs. (4) and (40) to obtain

$$
\frac{dH}{dN} = -\epsilon_H H,
$$

$$
\frac{d^2H}{dN^2} = -\epsilon_H(\epsilon_H + 2\delta_1)H. \qquad \text{(A3)}
$$

Integrating the Taylor expansion of H around N to find $\eta = \int_N^0 dN/e^N H$, we obtain

$$
aH\eta \approx 1 + \epsilon_H + 3\epsilon_H^2 + 2\epsilon_H\delta_1. \qquad \text{(A4)}
$$

Using this relation, the definition of f from Eq. (3), and the Hubble slow-roll hierarchy equation (40), we obtain for the GSR scalar parameters

$$
\ln f^2 \approx \ln\left(\frac{8\pi^2\epsilon_H}{H^2}\right) + 2\epsilon_H + 5\epsilon_H^2 + 4\epsilon_H\delta_1,
$$

$$
\frac{f'}{f} \approx -\delta_1 - 2\epsilon_H - 4\epsilon_H^2 - 3\epsilon_H\delta_1,
$$

$$
G' \approx 4\epsilon_H + 2\delta_1 + \frac{2}{3}\delta_2 + \frac{32}{3}\epsilon_H^2 + \frac{28}{3}\epsilon_H\delta_1 - \frac{2}{3}\delta_1^2,
$$

$$
G'' \approx -2\delta_2 - \frac{2}{3}\delta_3 - 8\epsilon_H^2 - 10\epsilon_H\delta_1 + 2\delta_1^2,
$$

$$
G^{(p)} \approx (-1)^{p+1}\left(2\delta_p + \frac{2}{3}\delta_{p+1}\right), \qquad (p > 2) \qquad \text{(A5)}
$$

and for the tensor parameters

$$
\ln f_h^2 \approx \ln\left(\frac{2\pi^2}{H^2}\right) + 2\epsilon_H + 5\epsilon_H^2 + 4\epsilon_H\delta_1,
$$

$$
\frac{f_h'}{f_h} \approx -\epsilon_H - 3\epsilon_H^2 - 2\epsilon_H\delta_1,
$$

$$
G_h' \approx 2\epsilon_H + \frac{22}{3}\epsilon_H^2 + \frac{16}{3}\epsilon_H\delta_1,
$$

$$
G_h'' \approx -4\epsilon_H^2 - 4\epsilon_H\delta_1,
$$

$$
G_h^{(p)} \approx 0, \qquad (p > 2). \qquad \text{(A6)}
$$

For the relationship with the potential parameters, we iteratively solve Eq. (48)

$$
\mathcal{U} = 2\epsilon_H + \mathcal{O}(N^{-2}),
$$

$$
\mathcal{V}_1 = \epsilon_H - \delta_1 - \frac{\delta_2}{3} + \mathcal{O}(N^{-2}) \qquad \text{(A7)}
$$

along with

$$
\mathcal{V}_p = -\frac{d\mathcal{V}_{p-1}}{dN} + \mathcal{O}(N^{-2})
$$

$$
= (-1)^p\left(\delta_p + \frac{\delta_{p+1}}{3}\right) + \mathcal{O}(N^{-2}) \qquad \text{(A8)}
$$

for $p \geq 2$. Notice that this is the same combination that enters into $G^{(p)}$ in Eq. (A5). Inverting these relations we obtain

$$
\epsilon_H = \frac{\mathcal{U}}{2} + \mathcal{O}(N^{-2}),
$$

$$
\delta_1 = \frac{\mathcal{U}}{2} - \sum_{n=0}^{\infty}\left(\frac{1}{3}\right)^n \mathcal{V}_{n+1} + \mathcal{O}(N^{-2}),
$$

$$
\delta_p = \sum_{n=0}^{\infty}\left(\frac{1}{3}\right)^n \mathcal{V}_{n+2} + \mathcal{O}(N^{-2}). \qquad \text{(A9)}
$$

We then plug these back into the exact Eqs. (47) and (48) and use

$$
\frac{V'}{V}\frac{d\mathcal{U}}{d\phi} = 2\mathcal{U}(\mathcal{V}_1 - \mathcal{U}),
$$

$$
\frac{V'}{V}\frac{d\mathcal{V}_p}{d\phi} = \mathcal{V}_{p+1} + [(p-1)\mathcal{V}_1 - p\mathcal{U}]\mathcal{V}_p, \qquad \text{(A10)}
$$

to obtain

$$\frac{3H^2}{V} \approx 1 + \frac{\mathcal{U}}{6} - \frac{\mathcal{U}^2}{12} + \frac{\mathcal{U}\mathcal{V}_1}{9},$$

$$\frac{\epsilon_H}{\mathcal{U}} \approx \frac{1}{2} - \frac{\mathcal{U}}{3} + \sum_{n=1}^{\infty} \left(\frac{1}{3}\right)^n \mathcal{V}_n + \frac{4}{9}\mathcal{U}^2 - \frac{5}{6}\mathcal{U}\mathcal{V}_1 + \frac{5\mathcal{V}_1^2}{18},$$

$$\delta_1 \approx \frac{\mathcal{U}}{2} - \sum_{n=0}^{\infty} \left(\frac{1}{3}\right)^n \mathcal{V}_{n+1} - \frac{2}{3}\mathcal{U}^2 + \frac{4}{3}\mathcal{U}\mathcal{V}_1 - \frac{\mathcal{V}_1^2}{3},$$

$$\delta_2 \approx \sum_{n=0}^{\infty} \left(\frac{1}{3}\right)^n \mathcal{V}_{n+2} + \mathcal{U}^2 - \frac{5}{2}\mathcal{U}\mathcal{V}_1 + \mathcal{V}_1^2,$$

$$\delta_p \approx (-1)^p \sum_{n=0}^{\infty} \left(\frac{1}{3}\right)^n \mathcal{V}_{n+p}, \qquad (p > 2) \qquad \text{(A11)}$$

where we have performed one more iteration of ϵ_H to obtain $\epsilon_H/\mathcal{U}$ to $\mathcal{O}(N^{-2})$ since it appears in the denominator of $\Delta_{\mathcal{R}}^2$.

As noted above, an advantage of the potential slow-roll parameters is that in the Taylor expansion for G' mixed p terms in δ_p go away when rewritten in $\mathcal{V}_p$,

$$G \approx \ln\left(\frac{V}{12\pi^2\mathcal{U}}\right) - \frac{7}{6}\mathcal{U} - \frac{21}{8}\mathcal{U}^2 + \frac{7}{3}\mathcal{U}\mathcal{V}_1 - \frac{1}{9}\mathcal{V}_1^2,$$

$$G' \approx 3\mathcal{U} - 2\mathcal{V}_1 + \frac{17}{6}\mathcal{U}^2 - \frac{5}{3}\mathcal{U}\mathcal{V}_1 - \frac{2}{3}\mathcal{V}_1^2,$$

$$G'' \approx -2\mathcal{V}_2 - 6\mathcal{U}^2 + 8\mathcal{U}\mathcal{V}_1,$$

$$G^{(p)} \approx -2\mathcal{V}_p, \qquad (p > 2), \qquad \text{(A12)}$$

for the scalars and

$$G_h \approx \ln\left(\frac{V}{6\pi^2}\right) - \frac{7}{6}\mathcal{U} - \frac{55}{24}\mathcal{U}^2 + \frac{17}{9}\mathcal{U}\mathcal{V}_1,$$

$$G_h' \approx \mathcal{U} + \frac{5}{2}\mathcal{U}^2 - 2\mathcal{U}\mathcal{V}_1,$$

$$G_h'' \approx -2\mathcal{U}^2 + 2\mathcal{U}\mathcal{V}_1,$$

$$G_h^{(p)} \approx 0, \qquad (p > 2), \qquad \text{(A13)}$$

for the tensors.

With these relations, the full $\mathcal{O}(N^{-2})$ expressions with $\Delta N \ll 1$ for the curvature power spectrum observables,

$$\ln\Delta_{\mathcal{R}}^2(k) \approx G(\ln x_f) + \sum_{p=1}^{\infty} q_p G^{(p)}(\ln x_f)$$

$$+ \frac{\pi^2}{8}[G'(\ln x_f)]^2 - 4\left[\frac{f'}{f}(\ln x_f)\right]^2,$$

$$n_s - 1 \approx -G'(\ln x_f) - \sum_{p=1}^{\infty} q_p G^{(p+1)}(\ln x_f),$$

$$\alpha \approx G''(\ln x_f) + \sum_{p=1}^{\infty} q_p G^{(p+2)}(\ln x_f), \quad \text{(A14)}$$

become

$$\Delta_{\mathcal{R}}^2 \approx \frac{V}{12\pi^2\mathcal{U}}\Big[1 + \left(3q_1 - \frac{7}{6}\right)\mathcal{U} - 2\sum_{p=1}^{\infty} q_p\mathcal{V}_p$$

$$+ \left(3q_2 - \frac{2}{3}q_1 - \frac{103}{9} + \frac{3\pi^2}{2}\right)\mathcal{U}^2$$

$$+ \left(-4q_2 + \frac{2}{3}q_1 + 15 - 2\pi^2\right)\mathcal{U}\mathcal{V}_1$$

$$+ \left(4q_2 - \frac{2}{3}q_1 - \frac{13}{3} + \frac{2\pi^2}{3}\right)\mathcal{V}_1^2\Big],$$

$$n_s \approx 1 - 3\mathcal{U} + 2\mathcal{V}_1 + 2\sum_{p=1}^{\infty} q_p\mathcal{V}_{p+1}$$

$$+ \left(6q_1 - \frac{17}{6}\right)\mathcal{U}^2 - \left(8q_1 - \frac{5}{3}\right)\mathcal{U}\mathcal{V}_1 + \frac{2}{3}\mathcal{V}_1^2,$$

$$\alpha \approx -2\mathcal{V}_2 - 2\sum_{p=1}^{\infty} q_p\mathcal{V}_{p+2} - 6\mathcal{U}^2 + 8\mathcal{U}\mathcal{V}_1. \qquad \text{(A15)}$$

The analogous relations for the tensor observables give

$$\Delta_{+,\times}^2 \approx \frac{V}{6\pi^2}\Big[1 + \left(q_1 - \frac{7}{6}\right)\mathcal{U}$$

$$+ \left(-q_2 + \frac{4}{3}q_1 - \frac{8}{3} + \frac{\pi^2}{6}\right)\mathcal{U}^2$$

$$+ \left(2q_2 - 2q_1 + \frac{17}{9}\right)\mathcal{U}\mathcal{V}_1\Big],$$

$$r \approx 8\mathcal{U} - 16q_1\mathcal{U}(\mathcal{U} - \mathcal{V}_1),$$

$$n_t \approx -\mathcal{U} + \left(2q_1 - \frac{5}{2}\right)\mathcal{U}^2 - 2(q_1 - 1)\mathcal{U}\mathcal{V}_1,$$

$$\alpha_t \approx -2\mathcal{U}(\mathcal{U} - \mathcal{V}_1). \qquad \text{(A16)}$$

These expressions can be used to derive any second-order approximation specified consistently by the order in the hierarchy of $q_p(\ln x_f)$ corrections or in the standard approach by keeping only $\mathcal{O}(1/N\Delta N)$ terms with $\ln x_f = 0$.

For example, in terms of the Hubble flow parameters of Eq. (46), keeping the conversions in the standard approach where we assume $\epsilon_n = \mathcal{O}(1/N)$ gives

$$n_s - 1 = -2\epsilon_1 - \epsilon_2 - 2\epsilon_1^2 + \left(2q_1 - \frac{11}{3}\right)\epsilon_1\epsilon_2$$

$$+ \left(q_1 - \frac{1}{3}\right)\epsilon_2\epsilon_3,$$

$$\alpha = -2\epsilon_1\epsilon_2 - \epsilon_2\epsilon_3,$$

$$n_t = -2\epsilon_1 - 2\epsilon_1^2 + \left(2q_1 - \frac{8}{3}\right)\epsilon_1\epsilon_2,$$

$$\alpha_t = -2\epsilon_1\epsilon_2, \qquad \text{(HSO)} \qquad \text{(A17)}$$

which reproduces the standard result used in the literature (e.g. [1, 6, 7]) with $q_1 = q_1(0) = 7/3 - \ln 2 - \gamma_E$. Note that because the truncation is inconsistent in the models we consider with $\Delta N \ll |N|$, these relations differ numerically from the SO approximation expressed in terms
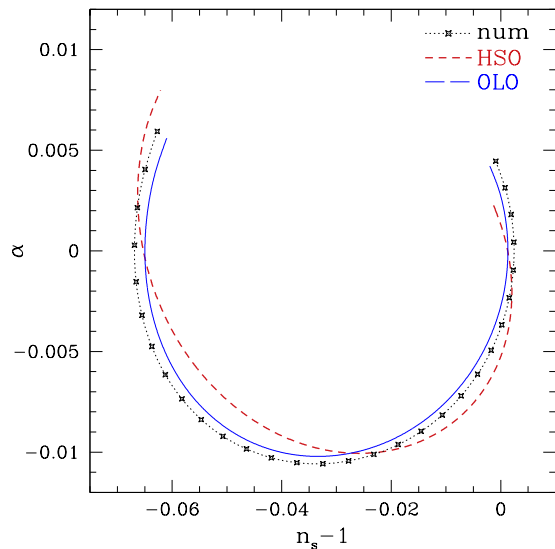
FIG. 14. Low frequency $\omega = 1/3$ oscillation trajectories in the n_s-α plane under the OLO and HSO approximations as in Fig. 8. HSO like SO provides an inconsistent trajectory and is worse than the simpler OLO approximation.

of the same truncation in the potential parameters in the text unless the potential is cubic. Nonetheless $n_s - 1$ and α are still inconsistently evaluated, and the Hubble flow second order (HSO) also performs worse than the simpler OLO approximation (see Fig. 14).

[1] P. Ade *et al.* (Planck Collaboration), (2015), arXiv:1502.02114 [astro-ph.CO].
[2] E. D. Stewart and D. H. Lyth, Phys.Lett. **B302**, 171 (1993), arXiv:gr-qc/9302019 [gr-qc].
[3] J. E. Lidsey, A. R. Liddle, E. W. Kolb, E. J. Copeland, T. Barreiro, *et al.*, Rev.Mod.Phys. **69**, 373 (1997), arXiv:astro-ph/9508078 [astro-ph].
[4] S. M. Leach, A. R. Liddle, J. Martin, and D. J. Schwarz, Phys.Rev. **D66**, 023515 (2002), arXiv:astro-ph/0202094 [astro-ph].
[5] M. Cortes, A. R. Liddle, and P. Mukherjee, Phys.Rev. **D75**, 083520 (2007), arXiv:astro-ph/0702170 [astro-ph].
[6] P. A. R. Ade *et al.* (Planck), Astron. Astrophys. **571**, A22 (2014), arXiv:1303.5082 [astro-ph.CO].
[7] D. Baumann, D. Green, and R. A. Porto, JCAP **1501**, 016 (2015), arXiv:1407.2621 [hep-th].
[8] Q. Gao, Y. Gong, T. Li, and Y. Tian, Sci.China Phys.Mech.Astron. **57**, 1442 (2014), arXiv:1404.7214 [hep-th].
[9] L. Boyle, K. M. Smith, C. Dvorkin, and N. Turok, Phys. Rev. **D92**, 043504 (2015), arXiv:1408.3129 [astro-ph.CO].
[10] S. Dodelson and E. Stewart, Phys. Rev. **D65**, 101301 (2002), arXiv:astro-ph/0109354.
[11] E. D. Stewart, Phys.Rev. **D65**, 103508 (2002), arXiv:astro-ph/0110322 [astro-ph].
[12] J.-O. Gong and E. D. Stewart, Phys.Lett. **B510**, 1 (2001), arXiv:astro-ph/0101225 [astro-ph].
[13] J. Choe, J.-O. Gong, and E. D. Stewart, JCAP **0407**, 012 (2004), arXiv:hep-ph/0405155.
[14] C. Dvorkin and W. Hu, Phys.Rev. **D81**, 023518 (2010), arXiv:0910.2237 [astro-ph.CO].
[15] J.-O. Gong, Class.Quant.Grav. **21**, 5555 (2004), arXiv:gr-qc/0408039 [gr-qc].
[16] W. Hu, Phys.Rev. **D89**, 123503 (2014), arXiv:1405.2020 [astro-ph.CO].
[17] E. Silverstein and A. Westphal, Phys.Rev. **D78**, 106003 (2008), arXiv:0803.3085 [hep-th].
[18] T. Kobayashi and F. Takahashi, JCAP **1101**, 026 (2011), arXiv:1011.3988 [astro-ph.CO].
[19] M. Czerny, T. Kobayashi, and F. Takahashi, (2014), 10.1016/j.physletb.2014.06.018, arXiv:1403.4589 [astro-ph.CO].
[20] P. D. Meerburg, Phys.Rev. **D90**, 063529 (2014), arXiv:1406.3243 [astro-ph.CO].
[21] R. Flauger, L. McAllister, E. Pajer, A. Westphal, and G. Xu, JCAP **1006**, 009 (2010), arXiv:0907.2916 [hep-th].
[22] R. Flauger, L. McAllister, E. Silverstein, and A. Westphal, (2014), arXiv:1412.1814 [hep-th].
[23] W. H. Kinney, Phys.Rev. **D72**, 023515 (2005), arXiv:gr-qc/0503017 [gr-qc].
[24] M. H. Namjoo, H. Firouzjahi, and M. Sasaki, Europhys.Lett. **101**, 39001 (2013), arXiv:1210.3692 [astro-ph.CO].
[25] J. Martin, H. Motohashi, and T. Suyama, Phys.Rev. **D87**, 023514 (2013), arXiv:1211.0083 [astro-ph.CO].
[26] H. Motohashi, A. A. Starobinsky, and J. Yokoyama, (2014), arXiv:1411.5021 [astro-ph.CO].
[27] K. Kadota, S. Dodelson, W. Hu, and E. D. Stewart, Phys.Rev. **D72**, 023510 (2005), arXiv:astro-ph/0505158 [astro-ph].
[28] W. Hu, Phys.Rev. **D84**, 027303 (2011), arXiv:1104.4500 [astro-ph.CO].
[29] C. Dvorkin and W. Hu, Phys.Rev. **D82**, 043513 (2010), arXiv:1007.0215 [astro-ph.CO].

[30] C. Dvorkin and W. Hu, Phys.Rev. **D84**, 063515 (2011), arXiv:1106.4016 [astro-ph.CO].

[31] V. Miranda, W. Hu, and C. Dvorkin, Phys.Rev. **D91**, 063514 (2015), arXiv:1411.5956 [astro-ph.CO].